

1 **Measured and modelled Cloud Condensation Nuclei (CCN)**
2 **concentration in São Paulo, Brazil: The importance of aerosol size-**
3 **resolved chemical composition on CCN concentration prediction**

4
5 G. P. Almeida¹, J. Brito², C. A. Morales³, M.. F. Andrade³, P. Artaxo²

6 1, State University of Ceará, Physics Department, Fortaleza, CE, Brazil. Email:
7 gerson.almeida@uece.br

8 2, University of São Paulo, Physics Institute, São Paulo, SP, Brazil

9 3, University of São Paulo, Astronomy, Geophysics and Atmospheric Science Institute,
10 São Paulo, SP, Brazil.

11
12 **Abstract**

13
14 Measurements of cloud condensation nuclei (CCN), aerosol size distribution and
15 non-refractory chemical composition were performed from 16 to 31 October 2012 in the
16 São Paulo Metropolitan Area (SPMA), Brazil. CCN measurements were performed at
17 0.23%, 0.45%, 0.68%, 0.90% and 1.13% water supersaturation and were subsequently
18 compared with Köhler theory, considering the chemical composition. Real-time
19 chemical composition has been obtained deploying for the first time in SPMA an
20 Aerosol Chemical Ionization Monitor (ACSM). CCN closure analyses were performed
21 considering internal mixtures.

22 Average aerosol composition during the studied period yielded (arithmetic mean
23 \pm standard deviation) 4.81 ± 3.05 , 3.26 ± 2.10 , 0.30 ± 0.27 , 0.52 ± 0.32 , 0.37 ± 0.21 and
24 $0.04 \pm 0.04 \mu\text{g m}^{-3}$ for organics, BC, NH_4 , SO_4 , NO_3 and Cl, respectively. Particle
25 number concentration was $12813 \pm 5350 \text{ cm}^{-3}$, with a dominant nucleation mode. CCN
26 concentrations were on average $1090 \pm 328 \text{ cm}^{-3}$ and $3570 \pm 1695 \text{ cm}^{-3}$ at SS=0.23%
27 and SS=1.13%, respectively.

1 Results show an increase in aerosol hygroscopicity in the afternoon as a result of
2 aerosol photochemical processing, leading to an enhancement of both organic and
3 inorganic secondary aerosols in the atmosphere, as well as an increase in aerosol
4 average diameter.

5 Considering the bulk composition alone, observed CCN concentrations were
6 substantially overpredicted when compared with Köhler theory ($44.1 \pm 47.9\%$ at 0.23%
7 supersaturation and $91.4 \pm 40.3\%$ at 1.13% supersaturation). Overall, the impact of
8 composition on the calculated CCN concentration (N_{CCN}) decreases with decreasing
9 supersaturation, partially because using bulk composition introduces less bias for large
10 diameters and lower critical supersaturations, defined as the supersaturation at which the
11 cloud droplet activation will take place. Results suggest that the consideration of only
12 inorganic fraction improves the calculated N_{CCN} .

13 Introducing a size-dependent chemical composition based on filter
14 measurements from previous campaigns has considerably improved simulated values
15 for N_{CCN} (average overprediction error $14.8 \pm 38.6\%$ at 0.23% supersaturation and $3.6 \pm$
16 21.6% at 1.13% supersaturation). This study provides the first insight on aerosol real-
17 time composition and hygroscopicity at a site strongly impacted by emissions of a
18 unique vehicular fleet due to the extensive biofuel usage.

19

1 **Introduction**

2

3 Cloud condensation nuclei (CCN) are a subset of atmospheric aerosol that
4 enable the condensation of water vapour and formation of cloud droplets when
5 submitted to a given level of water vapour supersaturation. The ability of a particle to
6 act as a CCN depends strongly on its size and chemical composition, which implies that
7 the knowledge of both parameters would suffice to provide an accurate prediction on
8 ambient CCN concentrations.

9 CCN are key elements of the hydrological cycle and climate on regional as well
10 as global scales. Elevated concentrations of CCN tend to increase the concentration of
11 cloud droplets in clouds and decrease their sizes, which may modify trends in rainfall
12 (Khain, 2009 and references therein). In addition to their cloud microphysical effects,
13 CCN also modulate cloud formation and convective behaviour through their radiative
14 effects. One of the largest uncertainties in the current understanding of climate change is
15 the response of cloud characteristics and precipitation processes to increasing aerosol
16 concentrations. Therefore, one of the central challenges in climate assessment is to
17 accurately describe the spatial distribution of CCN, its relative contribution from
18 anthropogenic activities, and the dependence of CCN efficiency on the aerosol size
19 distribution and chemical composition under atmospheric conditions (e.g. McFiggans et
20 al., 2006; IAPSAG, 2007; IPCC, 2007; Andreae and Rosenfeld, 2008).

21 Currently there is no consensus on how much detail on aerosol mixing state and
22 chemical composition is needed to predict N_{CCN} , which is expected to vary among
23 aerosol types and with the aging of atmospheric aerosols. Nevertheless, aerosol/CCN
24 closure has been achieved assuming simplified composition and an internal mixture in
25 some studies (e.g. Liu et al., 1996; Cantrell et al., 2001; Roberts et al., 2002; VanReken

1 et al., 2003, Rissler et al., 2004; Conant et al., 2004; Gasparini et al., 2006; Broekhuizen
2 et al., 2006; Ervens et al., 2007; Chang et al., 2007; Wang et al. 2008, Gunthe et al.,
3 2009; Shinozuka et al., 2009), while previous studies were largely unsuccessful (Bigg,
4 1986; Quinn et al., 1993; and Martin et al., 1994). Given the complex mixtures of
5 aerosol composition, with both inorganic and organic components, and the composition
6 dependency on aerosol size, a complete and rigorous description of aerosol
7 composition, mixing state and also their ability to act a CCN is a difficult task. As a
8 result, the representation of aerosol composition and mixing state in large scale models
9 is often greatly simplified. A common approximation, for example, is to consider
10 aerosols to be internally mixed, i.e., particles of any size are a mixture of all
11 participating species and have an identical composition. Nevertheless, such simplified
12 aerosol representation on atmospheric models can be significantly improved using an
13 efficient parameterization for the calculated N_{CCN} given the current measurements
14 techniques.

15 Megacities and large city-clusters are major source regions of atmospheric
16 particulate matter and its precursors, with regional and global impacts (Gurjar et al.,
17 2008). In recent years a number of studies were performed aiming to characterize the
18 CCN properties of the aerosol particles in urban environments and their effects on
19 regional air quality and climate (e.g. Matsumoto et al., 1997; Yum et al., 2005, 2007;
20 Broekhuizen et al., 2006; Kuwata et al., 2007, 2008, 2009; Wiedensohler et al., 2009;
21 Rose et al., 2010, 2011; Kuhn et al, 2010; Gunthe et al., 2011; Lance et al., 2013; Mei et
22 al., 2013).

23 Aiming to constrain aerosol sources, processing, and its impact on climate and
24 human health in the São Paulo Metropolitan Area (SPMA), the (*Narrowing the*
25 *Uncertainties in Aerosol aNd Climate changEes in the state of São Paulo*) has been

1 designed. With 20 million people and over 7 million vehicles using a blending of
2 gasoline with anhydrous ethanol (gasohol), pure ethanol, or diesel with biodiesel, the
3 SPMA is one of the largest urbanized regions on the planet. Furthermore, the region is
4 often impacted by industrial emissions (Albuquerque et al., 2012), thus resulting in a
5 complex suite of sources of aerosols and its precursors. Within the scope of the
6 NUANCE-SP project, aerosol and traces gases measurements were performed during
7 winter and spring of 2012 within the city of São Paulo.

8 In this study we report the first CCN measurements performed within the
9 SPMA. Furthermore, supporting measurements including real-time non-refractory
10 chemical speciation, aerosol size distribution and Black Carbon (BC) concentration
11 were performed. A comparison of modelled and observed N_{CCN} considering size
12 resolved chemical composition based on filter measurements from previous campaigns
13 has been performed as well.

14

15 **2 Experimental**

16

17 **2.1 Measuring site and meteorological conditions**

18

19 The SPMA is located at 23.5 ° S and 46.6 ° W, in the southeastern portion of
20 Brazil and consists of 39 highly urbanized and industrialized towns, among which is
21 included the city of São Paulo (Sánchez-Ccoyllo and Andrade, 2002). The urban site is
22 almost entirely located in the Sedimentary Basin of Tietê River, oriented from east to
23 west, with a mean elevation of 720 meters above sea level on an extensive floodplain.
24 This basin is bordered to the north by the Cantareira Hills, also oriented east to west and
25 with altitudes reaching up to 1200 meters. At the south-east side the valley is delimited
26 by Serra do Mar with altitudes generally exceeding 800 meters. SPMA is approximately

1 45 km from the Atlantic Ocean, holds about 0.1% of the Brazilian territory and is the
2 fourth largest urban conglomeration in the world. The climate is subtropical with dry
3 winters and wet summers (Oliveira et al., 2003). The measurements were made at the
4 Armando Salles de Oliveira campus of the University of São Paulo. The campus area is
5 a vast park, with an area of 7.4 km², without strong local sources. Thus, air masses
6 arriving at the station should be well mixed and make the measurements representative
7 of the ambient pollution burden of the city.

8 The instrumentation was set-up at the rooftop of the Pelletron particle beams
9 accelerator building, in the Physics institute of the University of São Paulo. The top of
10 the tower is about 40 meters above mean ground level. Three vertical sampling lines
11 with PM2.5 inlets mounted 1 m above the roof provided sample air to the instruments.
12 The sampling lines to the instruments were 3/8 inch stainless steel tubing with an inner
13 diameter of 1/4 inch from the inlet to the instruments and 2.2 m in length. Each
14 sampling line was exclusive for BC, chemical speciation, and size distribution (as well
15 as CCN) measurements. Besides the instrumentation for aerosol characterization, a
16 meteorological station (Lufft GmbH, model Ventus-200A) has been deployed as well.
17 During the study the weather was sunny with occasional precipitation. The average air
18 temperature and relative humidity (RH) for the whole period was 23.0 °C and 69%,
19 varying from 13.9 to 36.0 °C and from 96 down to 19%, respectively (Fig. 1). During
20 the period a moderately increase in the mean temperature was observed. Observations
21 suggest low wind intensities during the period.

22 Although originally planned, CCN measurements were not carried out
23 downstream of a Differential Mobility Analyzer (DMA) due to instrumental issues.
24 Such setup provides the activation fraction for a given aerosol dry diameter, allowing to
25 better assessing the role of the chemical composition.

1 Data presented in this study include aerosol size distribution, CCN spectra, BC
2 concentration and non-refractory chemical composition, measured from 16 to 31
3 October 2012, when we evaluated that the best combination of high quality data were
4 available. All measurements are reported at local ambient pressure and temperature
5 conditions. Local time (UTC minus 3 h) is used throughout this study. In the following
6 section a description of the instrumentation used is provided.

7 8 **2.2 Instrumentation**

9 10 **2.1 Cloud condensation nuclei counter (CCNC)**

11
12 A single-column continuous-flow stream-wise thermal gradient CCN chamber
13 (DMT CCNC-100, Roberts and Nenes, 2005, Lance et al., 2006) was used to measure
14 the total polydisperse CCN number concentration as a function of time and
15 supersaturation (SS). The effective water vapour supersaturation was regulated by the
16 temperature gradient applied between the upper and lower wetted end of the CCNC
17 flow column, where the activation takes place. Only particles having lower critical
18 supersaturation (SS_{crit}) than the SS in the column are activated and can grow into the
19 supermicron size-range. Droplets leaving the column are sized by an optical particle
20 counter (OPC) and counted as CCN if their diameter is larger than a threshold size of
21 $0.75 \mu\text{m}$.

22 The CCNC was operated at a total flow rate of 0.5 l min^{-1} with a sheath-to-
23 aerosol flow ratio of 10:1. One measurement cycle included measurements at 5 different
24 SS (0.20%, 0.40%, 0.60%, 0.80%, and 1.0%). The CCN concentration at each SS was
25 measured for 5 minutes, and we evaluated only the data produced after completely
26 adjustment to the supersaturation level.

1 For this dataset, factory calibration using $(\text{NH}_4)_2\text{SO}_4$ was applied, considering
2 recommended corrections from recent literature. Lance et al. (2006) has provided the
3 correction function in supersaturation for a given ambient pressure. Taking in account
4 that the system was originally calibrated in Boulder, Colorado (820 mbar) and deployed
5 in São Paulo (928 mbar), the correction factor is roughly 13%.

6 As such, the supersaturation levels measurements during our campaign were
7 estimated as 0.23%, 0.45%, 0.68%, 0.90%, and 1.13%.

8 To determine that the instrument was working correctly we considered the
9 temperatures presented by the instrument, the variation in CCN concentration according
10 to the related supersaturation, the amount of mass determined by ACSM, and the DMPS
11 aerosol spectra. In our analysis those factors were good enough for ensure the reliability
12 on the presented data.

14 **2.2. Differential Mobility Particle Sizer (DMPS) / Condensation Particle Counter** 15 **(CPC)**

16
17 A Differential Mobility Particle Sizer (DMPS) consisting of a bipolar charger, a
18 medium-long Vienna type DMA (Winklmayr et al., 1991) with a sample flow of 1.1
19 lpm and sheath flow of 6 lpm, and butanol based Condensation Particle Counter (CPC)
20 was used to measure number-size distribution of aerosol particles with diameters in the
21 range 10 – 500 nm. The CPC used for particle detection after the DMA was a 3010
22 model (TSI Inc., Shoreview, MN, USA). The CPC was calibrated for counting
23 efficiency as a function of particle size. During the measurements, the DMA was
24 operated in a stepwise scanning mode starting from 10 nm diameter and stepped
25 upwards or downward respectively. 22 diameter steps were used in the scans for a total
26 of 22 mobility channels. A single scan over the whole size range took 5 min. A CPC

1 (TSI 3772) was operated in parallel for comparison with particle number concentrations
2 from the DMPS. Based on such intercomparison, DMPS data has been corrected by a
3 factor of 1.12 to the whole campaign. Intercomparison has been performed for particle
4 numbers below 10000 cm^{-3} due to decreased accuracy in the CPC. Undercounting of
5 the DMPS may have been caused by slight deviations of the sample and sheath flow
6 rates from the nominal values, or a DMA transfer probability lower than assumed.

7

8 **2.3. A Multi-Angle Absorption Photometer (MAAP)**

9

10 Real-time BC mass concentration was measured using the Multi-Angle
11 Absorption Photometer (MAAP, Thermo Scientific model 5012). The instrument
12 measures simultaneously the optical attenuation and reflection of particles deposited on
13 a glass fibrous filter from several detection angles. By assuming an absorption
14 efficiency of $6.6 \text{ m}^2 \text{ g}^{-1}$ at 637nm, the instrument converts light absorption to BC
15 concentration (Petzold and Schönlinner, 2004; Müller et al., 2011).

16

17 **2.4 Aerosol Chemical Speciation Monitor (ACSM)**

18 An ACSM was used to provide real-time (30 min resolution) chemically
19 resolved mass concentrations of particulate ammonium, nitrate, sulphate, chloride, and
20 organic species in the submicron size range (Ng et al., 2011). The ACSM efficiently
21 samples aerosol particles through an aerodynamic lens in the 75-650 nm size ranges.
22 The focused particle beam is transmitted into a detection chamber where the non-
23 refractory fraction flash vaporizes on a hot oven (typically above 600°C). Subsequently,
24 evaporated gas phase compounds are ionized with 70eV electron impact and its
25 spectrum obtained using a quadrupole mass spectrometer. The chemical speciation is

1 determined via deconvolution of the mass spectra according the work described by
2 Allan et al. (2004).

3

4 **3. Results from Observations**

5

6 3.1 Measured aerosol and CCN activation properties

7 The time series of CCN number concentrations measured at different
8 supersaturations are shown in Figure 2a. As expected, CCN concentration increases
9 with supersaturation. CCN hourly mean number concentrations varied between 517 and
10 2291cm^{-3} at $SS=0.23\%$ and between 1191 and 10256cm^{-3} at $SS=1.13\%$ (highest SS)
11 with mean values and standard deviations of $1090 \pm 328\text{cm}^{-3}$ and $3570 \pm 1695\text{cm}^{-3}$,
12 respectively. Minimum and maximum observed CCN number concentrations at a
13 certain SS differed by a factor of four to one. The observed values are significantly
14 lower than those observed in the megacity region of Beijing (Gunthe et al., 2011).
15 Figure 2b shows the activated fraction, i.e., the ratio of the CCN number concentration
16 relative to the integrated DMPS number concentration. One interesting feature revealed
17 by Figure 2a is the low variability of CCN concentration activated at 0.23%. Even
18 during the large aerosol concentration event on the 16th October 2012, CCN
19 concentration does not exceed 2000cm^{-3} , showing an enhancement factor as high as 2.
20 Conversely, CCN concentration activated at 0.45% SS enhanced over four times during
21 the same event. A summary of CCN concentration observed during the period is shown
22 on table 1. Overall the activated fraction varied by a factor of $\sim 4 - 6$. The mean hourly
23 activated fraction is shown in Figure 2c. The activated fraction strongly decreases in the
24 morning hours, probably due to rush hour emission, consistent with observations of
25 Lance et al. (2013). Overall the activated fraction are under 0.4, with mean values of

1 0.10±0.05 for $SS=0.23\%$ and 0.29±0.15 for $SS=1.13\%$. Throughout the day, the
2 activated fraction increases, probably due to a combination of increase in average
3 diameter as well as production of secondary organic and inorganic aerosols. Mean
4 characteristics of the aerosol size distribution is shown in Figure 3. The aerosol size
5 distribution was most of the time monomodal, occasionally bimodal. Figure 3a depicts
6 such a feature for the pollution event for 16th October 2012. In many occasions it is
7 possible to see nucleation events occurring, as is observed at 7 and 9 hours, when a
8 large number of small particles below 40 nm are observed, as a result of fresh traffic
9 emission during morning hours. In the next few hours these particles seem to grow by
10 condensation, the size distribution becomes more peaked and shift to the right. On the
11 17th October (Figure 3b), the aerosol concentration was lower than those observed
12 during 16th October, and the nucleation process is not evident. The temporal evolution
13 of the mean aerosol concentration (CN) is also marked by the appearance of several
14 peaks that alternates with low CN values (Figure 3c). Given the strong coupling
15 between atmospheric processes, including aerosol growth and formation of secondary
16 aerosols, it is not observed a strong correlation between CN and N_{CCN} peaks throughout
17 the sampling period.

18 During the whole period the integrated number concentration varied between
19 3000 cm^{-3} and 27174 cm^{-3} , with a mean aerosol concentration of $12813 \pm 5350\text{ cm}^{-3}$
20 (Figure 3c). Fig. 3d shows the time series of aerosol number and volume mean
21 diameter, yielding an average value of 58nm for the former and 117nm for the latter.
22 The mean aerosol number concentration attained a maximum values at noon (Figure
23 3e), and decrease continuously after that. During observations a substantial fraction of
24 particles were present below $\sim 40\text{ nm}$ as was measured by the DMPS. The scrutiny of
25 the aerosol concentration data reveals that there is a lot of variation during the day as a

1 function of meteorological condition, but the general trends shown in Figure 3e is
2 maintained. The second quartile approaches the mean values and the standard deviation
3 is about the same for all hours of the day.

4 The bulk mass concentrations of ammonium, sulphate, nitrate and organics as
5 measured by the ACSM, are shown in Figure 4a, along with the BC mass
6 concentrations measured by the MAAP. Results are shown as 1 hour average.
7 Substantial variation on chemical composition was observed in the time-averaged
8 ACMS data. The balance of ammonium, nitrate and sulphate concentrations revealed
9 that the aerosol was far from being completely neutralized in many moments, especially
10 during the morning, which indicate that aerosol are relatively acidic and considerably
11 amount of sulphate can be in the form of ammonium bisulphate, as was also observed
12 by Quinn et al. (2006) and Middlebrook et al. (2012). During other time intervals, the
13 amount of NH_4 was above the amount needed for completely neutralization, and
14 sulphate are probably present as ammonium sulfate, as is shown on Figure 4b.

15 Figure 4c shows the mass fractions of the chemical components, listed in Table
16 2. The most abundant observed species were organics and BC, with a combined 86% of
17 all mass (49.3% and 36.9% for organics and BC, respectively), indicating the relevant
18 impact of diesel (heavy-duty) fuelled vehicle during the studied period. Other species
19 contributed with 5.6%, 4.3%, 3.4% and 0.4%, for SO_4 , NO_3 , NH_4 and Cl, respectively.
20 The relative contributions of Cl, NH_4 , NO_3 and SO_4 to the total mass fraction is
21 relatively small (less than 14% on average) but changes significantly during the days
22 (by a factor of 4) of the measurement period. Organic compounds and BC provide the
23 largest contribution to the total mass of aerosols, in agreement with previous studies in
24 the area (Ynoue et Andrade, 2004). Among the identified species, BC exhibited the
25 largest variability. In absolute terms, the mean hourly concentration of inorganics does

1 not exhibit a remarkable variation during the day. SO_4 , for example, ranges from 0.45
2 and $0.65 \mu\text{g m}^{-3}$. Organics, however, given the much higher ambient concentration, was
3 observed to span over a wider range of values throughout the day (from 3.5 up to 6.5
4 $\mu\text{g m}^{-3}$). In relative terms, however, both organics and inorganics present a comparable
5 variation during the day (45% and 30% relative to peak value, respectively). The
6 minimum values are observed at 08 hours local time, while the maximum values are
7 observed at 14 hours, as is shown in Figure 4d. The lower concentration value for the
8 organic fraction in aerosols seems to occur 1 hour later than those observed to the
9 aerosols number concentration. This is probably because the traffic emission results in
10 nucleation of aerosols in diameters lower than 40 nm, which are not measured by the
11 ACSM or low concentration of secondary organic aerosol. The mean concentration
12 observed during the whole period are 4.81 ± 3.05 , 3.26 ± 2.10 , 0.30 ± 0.27 , 0.52 ± 0.32 ,
13 0.37 ± 0.21 and $0.04 \pm 0.04 \mu\text{g m}^{-3}$ for organics, BC, NH_4 , SO_4 , NO_3 and Cl, respectively.

14 Considering still the data from the 16th and 17th October, one can observe that
15 activated fraction (Fig. 2b) decreases significantly when the inorganic fraction is
16 reduced (Fig. 4a), even when the aerosol concentration remains relatively large (Fig.
17 3c). Data analysis also indicates that the CCN concentration is much better correlated to
18 inorganic fraction than to aerosol concentration, which suggest that most of the high
19 variability of CCN number concentration is due to the variations of the chemical
20 composition, while a smaller part of it can be attributed to variability of the aerosol
21 properties such as shape of the size distribution and the total particle number
22 concentration.

23

24 **3.2 CCN modelling study and the sensitivity of calculated N_{CCN} to assumed aerosol** 25 **size dependence composition**

1

2 A particle's ability to act as CCN depends on its size and chemical composition.

3 In this study both particle number size distribution and chemical bulk composition data

4 are available. As such, supposing internal mixture of the species provided by ACSM

5 and a simplified Köhler theory, we determine the critical supersaturation a dry diameter

6 needs to be submitted to be activated. Köhler theory (Köhler, 1936) describes the

7 equilibrium saturation ratio, S , over an aqueous solution droplet. According to Köhler8 theory S is defined by the ratio of p , the partial vapour pressure, and p_0 , the saturation

9 vapour pressure of water, and can be written as

10
$$S = a_w \exp\left(\frac{4\sigma M_w}{RT\rho_w D_{drop}}\right) \quad (1)$$

11 where a_w is the water activity of the solution, ρ_w is the density of water, M_w is the12 molecular weight of water, σ_{sol} is the surface tension of the solution/air interface13 (considered constant and equals to the surface tension of water on this study, 0.072 J.m^{-2}),14 R is the universal gas constant, T is temperature, and D_{drop} is the diameter of the

15 droplet.

16 Following Petters and Kreidenweis (2007), we used a semi-empirical water

17 activity parameterization for definition of a_w

18
$$a_w = \left(1 + \kappa \frac{D_0^3}{D_{drop}^3 - D_0^3}\right)^{-1} \quad (2)$$

19

20 where κ is the hygroscopicity parameter, and D_0 the dry particle diameter. Substituting21 a_w in Eq. (1) with Eq. (2) provides the κ -Köhler equation:

22
$$S = \left(1 + \kappa \frac{D_0^3}{D_{drop}^3 - D_0^3}\right)^{-1} \exp\left(\frac{4\sigma M_w}{RT\rho_w D_{drop}}\right) \quad (3)$$

23 The SS_{crit} of a particle with properties (D_0, κ) corresponds to the maximum value of S 24 obtained with Eq. (3) considering D_{drop} as the independent variable. The SS_{crit} of any dry

1 diameter with known chemical composition can be determined by numerical iteration
2 considering variation on D_{drop} and determining the equivalent equilibrium saturation
3 rate.

4 The time resolved mass fractions defined above can be used to feed the equation
5 for $\kappa = f_{org}\kappa_{org} + f_{inor}\kappa_{inor}$ (Dusek et al., 2010; Rose et al., 2011) to get the
6 ACMS/MAAP derived κ as a function of time, where we use $\kappa_{org} = 0.1$, and $\kappa_{inor} =$
7 0.7 (Dusek et al., 2010). The mean ACSM /MAAP derived κ value for the period
8 studied was 0.15 ± 0.04 , from this values 0.10 ± 0.03 can be attributed to the inorganic
9 fraction, which imply that the largest variation experienced by κ is due to the variation
10 of the inorganic fraction. This value is lower than the global mean κ values for
11 continental regions (0.27 ± 0.21) and much lower than those value for marine regions
12 (0.72 ± 0.24) (Andreae and Rosenfeld, 2008; Pringle et al. 2010). This is a result of the
13 relatively low inorganic mass fraction. The mean κ values present their lowest values
14 around noon and their highest values after sunset.

15

16 3.2.1 Internal mixture and ACSM chemical composition

17

18 In this section we evaluate the relation of simulated and measured N_{CCN} . We
19 assume internal mixture of aerosol chemical composition derived from the ACSM, and
20 uses the aerosol size distribution determined by the DMPS to determine the N_{CCN} at a
21 given supersaturation.

22 Initially, the size-independent solubility value, κ_{si} , is determined using the values
23 of Dusek et al. (2010) ($\kappa=0.1$ for organics and $\kappa=0.7$ for inorganics, κ is considered zero
24 for BC). We then calculate the critical supersaturation for each diameter in the DMPS
25 using eq. (3) and κ_{si} . The total modelled CCN concentration for a given supersaturation

1 is determined integrating the DMPS derived particle number size distribution
2 considering those classes of diameters whose critical supersaturation are lower or equals
3 to the supersaturation under consideration. Since we have only 22 size channel for the
4 whole size distribution it is necessary to interpolate it in order to be able to integrate
5 properly.

6 The modelled results indicate an overestimation of N_{CCN} , with increasing
7 overestimation factor with supersaturation. The slope of the fitted line increases from
8 1.52 to 1.89 when going from 0.23% to 1.13% of supersaturation (Table 3a), shown on
9 Figure 5, while the correlation coefficients (R^2) tend to go from 0.44 to 0.79, showing
10 that the data scattering tends to decrease as the supersaturation increases and the
11 overestimation tends to be higher as the particle size decreases. The mean relation
12 between N_{CCN} simulated and observed was 1.44 ± 0.48 for 0.23% supersaturation and
13 1.91 ± 0.40 for 1.13% supersaturation. A lower error at lower supersaturation can be
14 expected due to the larger importance of particle size regarding particle chemical
15 composition when one considers larger sizes, as expected. Overall, the impact of
16 chemical composition on calculated N_{CCN} decreases with decreasing supersaturation,
17 partially because using bulk composition introduces less bias for larger sizes at lower
18 supersaturations, and also by the fact that aerosol mass determined by the ACSM is
19 most defined by the largest particles. In this case, the fraction of inorganics and organics
20 mass in larger particles approach that measured by ACSM.

21 It can also be shown that if a smaller solubility factor ($\kappa \sim 0.60$) is taken in to
22 account for the inorganic fraction, the modelled overestimation values are only slightly
23 smaller (less than 5%) than those shown in Table 3a.

1 Considering the assumptions of size-averaged chemical composition, particles
2 smaller than 40 nm do not affect the calculated CCN number concentration because
3 $D_{0,crit}$ at the 1.0% supersaturation was always above 40 nm.

4 A series of new simulations were performed varying the values of κ_{org} from 0.1
5 until 0.0, still considering internal mixing. The resulting overestimation becomes lower
6 and lower as long as κ_{org} decrease from 0.1 until 0.0. The slope of fitted lines decreased
7 to 1.27 and 1.52 for 0.23% and 1.13% supersaturation, respectively, when κ_{org} is set 0.
8 There is also an decrease on the mean ratio between modelled and observed N_{CCN} .
9 Values decreased to 1.21 ± 0.42 and 1.54 ± 0.33 for 0.23% and 1.13% supersaturation,
10 respectively.

12 3.2.2 Internal mixture and size dependent chemical composition

14 Also as part of NUANCE-SP project, a measurement campaign was performed
15 from 15th August to 5th September 2012, at the roof of the Institute of Astronomy,
16 Geophysics and Atmospheric Science (IAG), to chemically characterize aerosols from
17 SPMA. The building is about 150 meters far from the place where CCN and aerosol
18 measurements described above occurred. During this measurement campaign, aerosols
19 were collected using a Micro-Orifice Uniform Deposit Impactor (MOUDI, model 100;
20 MSP Corporation – Marple et al. 1986) once a day. The mass concentrations of the
21 MOUDI samples were obtained gravimetrically using an electronic high precision
22 microbalance with a sensitivity of 1 μg (Mettler-Toledo). Further analysis was
23 performed using particle-induced X-ray emission (PIXE) and, more recently, ion
24 chromatography, as described in Albuquerque et al. (2012), Vasconcellos et al. (2011)
25 and Sánchez-Ccoyllo and Andrade (2002).

1 Figure 6a illustrates the 24 hours mean mass distribution observed for the period.
2 It is shown that most of the mass distribution is observed between 180 and 320 nm.
3 Considering the four stages from 100 nm to 560 nm, the mean mass concentration
4 sampled during the period of MOUDI operation was $10.9 \pm 6.3 \mu\text{g}/\text{m}^3$, which was
5 comparable to the one evaluated by the ACSM and MAAP described above (8.9 ± 6.0
6 $\mu\text{g}/\text{m}^3$). Values are in good agreements with the previous work (Albuquerque et al.,
7 2012; Vasconcellos et al., 2011; and Sánchez-Ccoyllo and Andrade, 2002) that have
8 shown a size dependency of inorganic concentration matter in Sao Paulo. The work of
9 Vasconcellos et al. (2011), for example, has shown that sulphate, nitrate, ammonium,
10 calcium and sodium are the most abundant water-soluble ions in São Paulo. Analysis
11 from 15th August to 5th September 2012 clearly show that sulphate is a major
12 component of the accumulation mode (diameters larger than 180 nm), as is also shown
13 in Figure 6a, but values are largely variable. At 100 nm the fraction of Sulphate (Figure
14 6b) varied from 5.8% to 17.4%, which depress the critical supersaturation of particles
15 with this size (from 0.5 to 0.3% considering only the contribution of $(\text{NH}_4)_2\text{SO}_4$).

16 For diameters smaller than 100 nm the fraction of sulphate decreases
17 systematically, and one observes a value of about 2.5% at 20 nm. In some occasion,
18 nevertheless, an increased in sulphate fraction was seen at 50 nm, which produces a
19 relatively large mean value for that size. Considering only the contribution of
20 $(\text{NH}_4)_2\text{SO}_4$, the variation of the critical supersaturation for particles of this size range
21 would be from 0.7 (~ 7% of $(\text{NH}_4)_2\text{SO}_4$) to 1.2% (~ 23% of $(\text{NH}_4)_2\text{SO}_4$), which suggests
22 that particles around 50 nm are the lower limit size range for activation on this study.

23 Considering the large fraction of sulphate in the accumulation mode and the
24 large fraction of organic compounds on total aerosol mass, one can argue that organic

1 compound is predominant at smaller particles. One can also conclude that particles in
2 the nucleation or Aitken size range were composed mostly of organics.

3 By observing that exist an aerosol chemical size dependency of inorganics, it is
4 possible to improve the N_{CCN} modeling. Considering that mass distribution observed by
5 MOUDI was shown to be consistent with Aerosol Mass Spectrometer (AMS) data
6 (Zhang et al., 2005), we assume that the inorganic size fraction during the CCN
7 measurement period takes the same mean size dependency as observed for sulphate
8 during measurements taken from 15th August to 5th September 2012. It is worth to say
9 that CCN closure utilizing AMS measurements tend to be more successful (typically
10 within 20–50 %), due to its fast time resolution (1 Hz) and ability to resolve size-
11 dependent composition. CCN closures in remote environments that use filter-based
12 methods have nevertheless given good closure, on the order of a few percent
13 (Bougiatioti et al., 2009, 2011).

14 The time resolved mass fractions defined above can be used to feed the equation
15 for κ considering a variation with size as a function of time. For this propose we
16 distributed the total inorganic mass from ACSM at a given time through all sizes using a
17 polynomial function fitted through the points that represent the size-resolved sulfate
18 mass fraction (Figure 6b) and also ensure mass conservation.

19 Strictly, the polynomial function defined above can only be applied from 75 nm
20 to 650 nm. However, the application to particles with diameter smaller the 75 nm does
21 not add large errors to the procedure, since usually there is only a small amount of mass
22 below this size range. For particles larger than about 250 nm, the procedure does not
23 modify significantly the critical supersaturation, once at this diameter range the size is
24 more important than chemical composition.

1 The new modelled results are presented on Figure 7. The results of the size-
2 dependent simulations are shown in Table 3.b. Result show that when we use the
3 inorganic fraction furnished by MOUDI+PIXE analysis there is a reduction on the slope
4 of fitted lines for the comparison of modelled and observed N_{CCN} for all supersaturation.
5 For 0.23% supersaturation, for example, the slope is 1.22, with $R^2=0.43$, indicates a
6 better agreement than when the mean values furnished by ACSM is considered on the
7 simulation. It is also observed a reduction on the mean relation between modelled and
8 observed CCN, given now by 1.14 ± 0.39 . There is a reduction on the slope for all fitted
9 lines relating simulated and observed N_{CCN} . For the case of 1.13% supersaturation, the
10 slope of fitted line is 1.03 with $R^2=0.79$, with mean relation between modelled and
11 observed CCN of 1.04 ± 0.22 . For this particular assumption, $D_{0,crit}$ at the 1.13%
12 supersaturation was most of the time above 65 nm, with mean value of 68 nm.

13 Considering any k_{org} different from 0.0 imply increasing overestimation of
14 N_{CCN} for all supersaturation. The overestimation, obviously, increases systematically for
15 increasing supersaturation.

16 These results shows that the measured number distribution of the DMPS,
17 combined with the chemical composition information provided by the ACSM and the
18 mean chemical fraction information of the MOUDI+PIXE analysis, provides a reliable
19 estimate of CCN concentration.

20

21 3.2.3 Further improvement on the estimation of N_{CCN}

22

23 As previously stated, CCN closure utilizing AMS measurements tend to be more
24 successful due to its fast time resolution and ability to resolve size-dependent
25 composition. The use of mean values of MOUDI data although can significantly

1 improve the estimation of N_{CCN} induce systematic bias as a function time of the day for
2 all supersaturation. The results are shown in Figure 8 where we can see the mean
3 relation between modelled and measured N_{CCN} as a function of the time of the day.
4 From 7 hours to noon local time, for example, the N_{CCN} modelled clearly overestimate
5 observation, while an opposing tendency occurs during the afternoon. It can be
6 concluded that the mean mass partition presented by MOUDI analysis underestimates
7 the soluble fraction during the morning and overestimates it during the afternoon.
8 Castanho and Artaxo (2001) found that 40% of Fine particles were explained by
9 Organic Carbon (OC) and Ynoue and Andrade (2004) found for data collected in 1999
10 that OC explained 25% during the day and 43% at night of fine particles. Considering
11 that previous analysis have shown that the inorganic fraction tends to be higher during
12 the day than during the evening in São Paulo, only a higher resolution (~6 hours)
13 MOUDI analysis could probably allow the study and parameterization of the aerosol
14 soluble fraction as a function of size and time of day.

15

16 **Conclusions**

17

18 Aerosol measurements in São Paulo city showed that the urban area is a strong
19 source of aerosol particles. These particles can act as CCN and show large variability.
20 Minimum and maximum observed CCN number concentrations at a given SS differed
21 by a factor of four to one and suggest that chemical composition is the main factor
22 controlling the fraction of aerosols that can act as CCN.

23 The hygroscopicity range was substantially lower than that proposed for
24 continental sites (Andreae and Rosenfeld, 2008), likely due to the higher mass fraction

1 of organics. It was also observed that traffic emissions modulate the concentration of
2 aerosols, organic fraction and CCN efficiency.

3 The impact of k_{org} on calculated N_{CCN} concentration was examined calculating
4 N_{CCN} for different k_{Org} values (0.1, 0.07, 0.05, 0.03 and 0.00). Particle hygroscopicity
5 was computed from the bulk composition (i.e., derived from ACSM measurements)
6 using Eq. (3). Based on the particle hygroscopicity and k -Kohler theory, the critical
7 supersaturation was derived for each particle dry diameter (D_0). The N_{CCN} at the five
8 supersaturations were then computed from D_0 and the measured dry particle size
9 distributions. Results suggest that taking organic fraction in to account on the particles
10 hygroscopicities only increases the overestimation of modeled N_{CCN} regarding
11 observations.

12 Results show an increase in aerosol hygroscopicity in the afternoon as a result of
13 aerosol photochemical processing, leading to an enhancement of both organic and
14 inorganic secondary aerosols in the atmosphere, as well as an increase in aerosol
15 average diameter.

16 Our study suggests that the prediction of N_{CCN} can be achieved with an error of
17 about $\pm 24\%$ considering a mean size-dependent soluble fraction based on
18 MOUDI+PIXE analysis. The knowledge of the soluble salt fraction is sufficient for
19 description of CCN activity at São Paulo, which is consistent with other closure studies
20 conducted in the past.

21 The results from these measurements can be used to constrain the uncertainty
22 associated with assumptions in GCM modelling studies of the aerosol indirect effect. As
23 suggested in recent study (Sotiropoulou et al., 2007) if the CCN prediction error is on
24 the order of 20% it may not contribute a significant source of error in the assessment of
25 the aerosol indirect effect.

1

2 Acknowledgment. This research was funded from FAPESP (São Paulo Science
3 Foundation).

4

5 **References**

6

7 Albuquerque, T.T, Andrade, M. F., Ynoue, R. Y., 2012. Characterization of
8 atmospheric aerosols in the city of São Paulo, Brazil: comparisons between polluted and
9 unpolluted periods. *Environ. Monit. Assess*, 184 (2): 969-84. DOI: 10.1007/s10661-
10 011-2013-y.

11 Allan, J. D., Delia, A. E., Coe, H., Bower, K. N., Alfarra, M. R., Jimenez, J. L.,
12 Middlebrook, A. M., et al., 2004. A generalised method for the extraction of chemically
13 resolved mass spectra from Aerodyne aerosol mass spectrometer data. *Journal of*
14 *Aerosol Science*, 35(7), 909–922. doi:10.1016/j.jaerosci.2004.02.007

15 Andreae, M. O. and Rosenfeld, D., 2008. Aerosol-cloud-precipitation
16 interactions. Part 1. The nature and sources of cloud-active aerosols, *Earth Sci. Rev.*, 89,
17 13–41. *Atmos. Chem. Phys.*, 9, 7551–7575, doi:10.5194/acp-9-7551-2009.

18 Bigg, E. K.: Discrepancy between observation and prediction of concentrations
19 of cloud condensation nuclei, *Atmos. Res.*, 20,82–86, 1986.

20 Bougiatioti, A., Fountoukis, C., Kalivitis, N., Pandis, S. N., Nenes, A., and
21 Mihalopoulos, N.: Cloud condensation nuclei measurements in the marine boundary
22 layer of the Eastern Mediterranean: CCN closure and droplet growth kinetics, , 2009.
23 *Atmos. Chem. Phys.*, 9, 7053–7066, doi:10.5194/acp-9-7053-2009.

24 Bougiatioti, A., Nenes, A., Fountoukis, C., Kalivitis, N., Pandis, S. N., and
25 Mihalopoulos, N.: Size-resolved CCN distributions and activation kinetics of aged

1 continental and marine aerosol, 2011. *Atmos. Chem. Phys.*, 11, 8791–8808,
2 doi:10.5194/acp-11-8791-2011.

3 Broekhuizen, K., Chang, R.Y.-W., Leaitch, W. R., Li, S.-M., and
4 Abbatt, J. P. D., 2006. Closure between measured and modeled cloud condensation
5 nuclei (CCN) using size-resolved aerosol compositions in downtown Toronto, *Atmos.*
6 *Chem. Phys.*, 6, 2513-2524, doi:10.5194/acp-6-2513-2006.

7 Cantrell, W., Shaw, G., Cass, G. R., et al., 2001: Closure between aerosol
8 particles and cloud condensation nuclei at Kaashidhoo Climate Observatory, *J.*
9 *Geophys. Res.*, 106, 28711–28718, 2001.

10 Castanho A., Artaxo P., 2001: Wintertime and summertime São Paulo aerosol
11 source apportionment study. *Atmospheric Environment*, 35, 4889-4902.

12 CETESB – Companhia de Tecnologia de Saneamento Ambiental. Relatório
13 Anual de Qualidade do Ar no Estado de São Paulo 2006. São Paulo, 2007.

14 Chang, R. Y. W., Liu, P. S. K., Leaitch, W. R., and Abbatt, J. P.D., 2007.
15 Comparison between measured and predicted CCN concentrations at Egbert, Ontario:
16 Focus on the organic aerosol fraction at a semi-rural site, *Atmos. Environ.*, 41, 8172–
17 8182.

18 Conant, W. C., VanReken, T. M., Rissman, T. A., et al. , 2004. Aerosol-Cloud
19 Drop Concentration Closure in Warm Cumulus. *J. Geophys. Res.*, 109, D13204,
20 doi:10.1029/2003JD004324.

21 Dusek, U., G. P. Frank, J. Curtius, F. Drewnick, J. Schneider, A. Kürten, D.
22 Rose, M. O. Andreae, S. Borrmann, and U. Pöschl, 2010. Enhanced organic mass
23 fraction and decreased hygroscopicity of cloud condensation nuclei (CCN) during new
24 particle formation events, *Geophys. Res. Lett.*, 37, L03804, doi:10.1029/2009GL
25 040930.

1 Ervens, B., Cubison, M., Andrews, E., et al. , 2007. Prediction of cloud
2 condensation nucleus number concentration using measurements of aerosol size
3 distributions and composition and light scattering enhancement due to humidity, *J.*
4 *Geophys. Res.*, 112, D10S32, doi:10.1029/2006JD007426.

5 Gasparini, R., Li, R. J., Collins, D. R., et al. , 2006. Application of aerosol
6 hygroscopicity measured at the Atmospheric Radiation Measurement Program's
7 Southern Great Plains site to examine composition and evolution, *J. Geophys. Res.*,
8 111, D05S12, doi:10.1029/2004JD005448.

9 Gunthe, S. S., King, S. M., Rose, D., Chen, Q., Roldin, P., Farmer, D. K.,
10 Jimenez, J. L., Artaxo, P., Andreae, M. O., Martin, S. T., and Poschl, U. , 2009. Cloud
11 condensation nuclei in pristine tropical rainforest air of Amazonia: size-resolved
12 measurements and modeling of atmospheric aerosol composition and CCN activity,
13 Gunthe, S. S., Rose, D., Su, H., Garland, R. M., Achtert, P., Nowak, A.,
14 Wiedensohler, A., Kuwata, M., Takegawa, N., Kondo, Y., Hu, M., Shao, M., Zhu, T.,
15 Andreae, M. O., and Pöschl, U.: Cloud condensation nuclei (CCN) from fresh and aged
16 air pollution in the megacity region of Beijing, *Atmos. Chem. Phys.*, 11, 11023–11039,
17 doi:10.5194/acp-11-11023-2011, 2011. 15721, 15723

18 Gurjar, B., Butler, T., Lawrence, M., and Lelieveld, J.: Evaluation of emissions
19 and air quality in megacities, *Atmospheric Environment*, 42, 1593–1606, doi:
20 10.1016/j.atmosenv.2007.10.048, 2008.

21 Hänel, G.: Radiation budget of the boundary layer: Part II. Simultaneous
22 measurement of mean solar volume absorption and extinction coefficients of particles,
23 *Beitr. Phys. Atmos.*, 60, 241–247, 1987.

24 Köhler, H.: The nucleus in and the growth of hygroscopic droplets. *Trans.*
25 *Faraday Soc.*, 32, 1152–1161, 1936.

1 Kuhn, U., Ganzeveld, L., Thielmann, A., Dindorf, T., Schebeske, G., Welling,
2 M., Sciare, J., Roberts, G., Meixner, F. X., Kesselmeier, J., Lelieveld, J., Kolle, O. ,
3 Ciccioli, P., Lloyd, J., Trentmann, J., Artaxo, P. , and Andreae, M. O.: Impact of
4 Manaus City on the Amazon Green Ocean atmosphere: ozone production, precursor
5 sensitivity and aerosol load. *Atmos. Chem. Phys.*, 10, 9251–9282, 2010,
6 doi:10.5194/acp-10-9251-2010.

7 Kuwata, M., Kondo, Y., and Takegawa, N.: Critical condensed mass for
8 activation of black carbon as cloud condensation nuclei in Tokyo, *J. Geophys. Res.*,
9 114, D20202, doi:10.1029/2009JD012086, 2009.

10 Kuwata, M., Kondo, Y., Miyazaki, Y., Komazaki, Y., Kim, J. H., Yum, S. S.,
11 Tanimoto, H., and Matsueda, H.: Cloud condensation nuclei activity at Jeju Island,
12 Korea in spring 2005, *Atmos. Chem. Phys.*, 8, 2933–2948, doi:10.5194/acp-8-2933-
13 2008,2008.

14 Kuwata, M., Kondo, Y., Mochida, M., Takegawa, N., and Kawamura, K.:
15 Dependence of CCN activity of less volatile particles on the amount of coating observed
16 in Tokyo, *J. Geophys. Res.*, 112, D11207, doi:10.1029/2006JD007758, 2007.

17 Lance, S., Raatikainen, T., Onasch, T., Worsnop, D. R., Yu, X.-Y., Alexander,
18 M. L., Stolzenburg, M. R., McMurry, P. H., Smith, J. N., and Nenes, A.: Aerosol
19 mixing-state, hygroscopic growth and cloud activation efficiency during MIRAGE
20 2006. *Atmos. Chem. Phys.*, 13, 5049–5062, 2013. doi:10.5194/acp-13-5049-2013.

21 Liu, P. S. K., Leitch, W. R., Banic, C. M., et al., 1996. Aerosol observations at
22 Chebogue Point during the 1993 North Atlantic Regional Experiment: Relationships
23 among cloud condensation nuclei, size distribution, and chemistry, *J. Geophys. Res.*,
24 101, 28971–28990.

1 Marple, V. A., Rubow, K. L., Ananth, G. P., and Fissan, H. J. (1986). Micro-
2 orifice uniform impactor. *Journal of Aerosol Science*, 17, 489–494.

3 Martin, G. M., Johnson, D. W., and Spice, A.: The measurement and
4 parameterization of effective radius of droplets in warm stratocumulus clouds, *J. Atmos.*
5 *Sci.*, 51, 1823–1842, 1994.

6 Matsumoto, K., Tanaka, H., Nagao, I., and Ishizaka, Y.: Contribution of
7 particulate sulfate and organic carbon to cloud condensation nuclei in the marine
8 atmosphere, *Geophys. Res. Lett.*, 24,655–658, 1997.

9 McFiggans, G., Artaxo, P., Baltensperger, U., Coe, H., Facchini, M. C.,
10 Feingold, G., Fuzzi, S., Gysel, M., Laaksonen, A., Lohmann, U., Mentel, T. F., Murphy,
11 D. M., O’Dowd, C. D., Snider, J. R., and Weingartner, E., 2006: The effect of physical
12 and chemical aerosol properties on warm cloud droplet activation, *Atmos. Chem. Phys.*,
13 6, 2593–2649, doi:10.5194/acp-6-2593-2006.

14 Mei, F., Setyan, A., Zhang, Q., and Wang, J.: CCN activity of organic aerosols
15 observed downwind of urban emissions during CARES, 2013. *Atmos. Chem. Phys.*
16 *Discuss.*, 13, 9355-9399, doi:10.5194/acpd-13-9355-2013.

17 Middlebrook, A.M., Bahreini, R., Jimenez, J.L. and Canagaratna, M.R. (2012).
18 Evaluation of composition dependent Collection Efficiencies for the Aerodyne Aerosol
19 Mass Spectrometer Using Field Data. *Aerosol Sci. Technol.* 46: 258–271.

20 Müller, T., Henzing, J. S., de Leeuw, G., Wiedensohler, A., Alastuey, A.,
21 Angelov, H., Bizjak, M., Collaud Coen, M., Engström, J. E., Gruening, C., Hillamo, R.,
22 Hoffer, A., Imre, K., Ivanow, P., Jennings, G., Sun, J. Y., Kalivitis, N., Karlsson, H.,
23 Komppula, M., Laj, P., Li, S.-M., Lunder, C., Marinoni, A., Martins dos Santos, S.,
24 Moerman, M., Nowak, A., Ogren, J. A., Petzold, A., Pichon, J. M., Rodriguez, S.,
25 Sharma, S., Sheridan, P. J., Teinila, K., Tuch, T., Viana, M., Virkkula, A., Weingartner,

1 E., Wilhelm, R., and Wang, Y. Q., 2011: Characterization and intercomparison of
2 aerosol absorption photometers: result of two intercomparison workshops, *Atmos.*
3 *Meas. Tech.*, 4, 245–268, doi:10.5194/amt-4-245-2011.

4 Ng, N. L., Herndon, S. C., Trimborn, a., Canagaratna, M. R., Croteau, P. L.,
5 Onasch, T. B., Sueper, D., et al., 2011. An Aerosol Chemical Speciation Monitor
6 (ACSM) for Routine Monitoring of the Composition and Mass Concentrations of
7 Ambient Aerosol. *Aerosol Science and Technology*, 45(7), 780–794.
8 doi:10.1080/02786826.2011.560211

9 Padró, L. T., Moore, R. H., Zhang, X., Rastogi, N., Weber, R. J., and Nenes, A.:
10 Mixing state and compositional effects on CCN activity and droplet growth kinetics of
11 size-resolved CCN in an urban environment. *Atmos. Chem. Phys.*, 12, 10239–10255,
12 2012.doi:10.5194/acp-12-10239-2012.

13 Petters, M. D. and Kreidenweis, S. M., 2007: A single parameter representation
14 of hygroscopic growth and cloud condensation nucleus activity, *Atmos. Chem. Phys.*, 7,
15 1961-1971, doi:10.5194/acp-7-1961-2007.

16 Petzold, A. and Schönlinner, M., 2004. Multi-angle absorption photometry – a
17 new method for the measurement of aerosol light absorption and atmospheric black
18 carbon, *J. Aerosol Sci.*, 35, 421–441.

19 Petzold, A., Schloesser, M., Sheridan, P. J., Arnott, W. P., Ogren, J. A., and
20 Virkkula, A.: Evaluation of multi-angle absorption photometry for measuring aerosol
21 light absorption, *Aerosol Sci. Tech.*, 39, 40–51, 2005.

22 Pringle, K. J., Tost, H., Pozzer, A., Pöschl, U., and Lelieveld, J.: Global
23 distribution of the effective aerosol hygroscopicity parameter for CCN activation,
24 *Atmos. Chem. Phys.*, 10, 5241–5255, doi:10.5194/acp-10-5241-2010, 2010.

1 Quinn, P. K., Covert, D. S., Bates, T. S., Kapustin, V. N., Ramsey-Bell, D. C.,
2 and McInnes, L. M.: Dimethylsulfide/cloud condensation nuclei/climate system:
3 relevant size-resolved measurements of the chemical and physical properties of
4 atmospheric aerosol particles, *J. Geophys. Res.*, 98, 10 411–10 427, 1993.

5 Quinn, P. K., et al. (2006), Impacts of sources and aging on submicrometer
6 aerosol properties in the marine boundary layer across the Gulf of Maine, *J. Geophys.*
7 *Res.*, 111, D23S36, doi:10.1029/2006JD007582.

8 Rissler, J., Swietlicki, E., Zhou, J., Roberts, G., Andreae, M. O., Gatti, L. V., and
9 Artaxo, P. , 2004. Physical properties of the submicrometer aerosol over the Amazon
10 rain forest during the wet to-dry season transition – comparison of modeled and
11 measured CCN concentrations, *Atmos. Chem. Phys.*, 4, 2119–2143, doi:10.5194/acp-4-
12 2119-2004.

13 Roberts, G. C., Artaxo, P., Zhou, J. C., et al., 2002: Sensitivity of CCN spectra
14 on chemical and physical properties of aerosol: A case study from the Amazon Basin, *J.*
15 *Geophys. Res.*, 107, 8070, doi:10.1029/2001JD000583, 2002.

16 Rose, D., Gunthe, S. S., Su, H., Garland, R. M., Yang, H., Berghof, M.,
17 Cheng, Y. F., Wehner, B., Achtert, P., Nowak, A., Wiedensohler, A., Takegawa, N.,
18 Kondo, Y., Hu, M., Zhang, Y., Andreae, M. O., and Pöschl, U.: Cloud condensation
19 nuclei in polluted air and biomass burning smoke near the mega-city Guangzhou, China
20 – Part 2: Size-resolved aerosol chemical composition, diurnal cycles, and externally
21 mixed weakly CCN-active soot particles, *Atmos. Chem. Phys.*, 11, 2817-2836,
22 doi:10.5194/acp-11-2817-2011, 2011.

23 Sánchez-Ccoyllo, O.R, Andrade, M. F., 2002. The influence of meteorological
24 conditions on the behavior of pollutants concentrations in São Paulo, Brazil.
25 *Environmental Pollution*, 116, 257–263

1 Shinozuka, Y., Clarke, A. D., DeCarlo, P. F., Jimenez, J. L., Dunlea, E. J.,
2 Roberts, G. C., Tomlinson, J. M., Collins, D. R., Howell, S. G., Kapustin, V. N.,
3 McNaughton, C. S., and Zhou, J., 2009. Aerosol optical properties relevant to regional
4 remote sensing of CCN activity and links to their organic mass fraction: airborne
5 observations over Central Mexico and the US West Coast during MILAGRO/INTEX-B,
6 *Atmos. Chem. Phys.*, 9, 6727–6742, doi:10.5194/acp-9-6727-2009, 2009.

7 Sotiropoulou, R. E. P., Nenes, A., Adams, P. J., and Seinfeld, J.H.: Cloud
8 condensation nuclei prediction error from application of Köhler theory, 2007.
9 Importance for the aerosol indirect effect, *J. Geophys. Res.*, 112, D12202,
10 doi:10.1029/2006JD007834, 2007.

11 VanReken, T. M., Rissman, T. A., Roberts, G. C., et al. , 2003. Toward
12 aerosol/cloud condensation nuclei (CCN) closure during CRYSTAL-FACE, *J Geophys.*
13 *Res.*, 108, 4633, doi:10.1029/2003JD003582.

14 Vasconcellos, P. C., Souza, D. Z., G. A. Simone, Araújo, M. P., Naoto, E.,
15 Nascimento, K. H., Cavalcante, F. S., Santos, M., Smichowski, P., and Behrentz, E.,
16 2011. Comparative study of the atmospheric chemical composition of three South
17 American cities. *Atmos. Env.*, 45, 5770 – 5777.

18 Wang, J., Lee, Y. N., Daum, P. H., Jayne, J., and Alexander, M. L., 2008.
19 Effects of aerosol organics on cloud condensation nucleus (CCN) concentration and
20 first indirect aerosol effect, *Atmos. Chem. Phys.*, 8, 6325–6339, doi:10.5194/acp-8-
21 6325-2009.

22 Wiedensohler, A., Cheng, Y. F., Nowak, A., Wehner, B., Achtert, P., Berghof,
23 M., Birmili, W., Wu, Z. J., Hu, M., Zhu, T., Takegawa, N., Kita, K., Kondo, Y., Lou, S.
24 R., Hofzumahaus, A., Holland, F., Wahner, A., Gunthe, S. S., Rose, D., Su, H., and
25 Pöschl, U.: Rapid aerosol particle growth and increase of cloud condensation nucleus

1 activity by secondary aerosol formation and condensation: A case study for regional air
 2 pollution in northeastern China, *J. Geophys. Res.*, 114, D00G08, doi: 10.1029/2008
 3 JD010884, 2009.

4 Winklmayr, W., Reischl, G. P., Lindner, A. O., and Berner, A.: A new
 5 electromobility spectrometer for the measurement of aerosol size distributions in the
 6 size range from 1 to 1000 nm, *J. Aerosol Sci.*, 22, 289–296, 1991.

7 Ynoue, R. Y., and Andrade, M.F. Size-Resolved Mass Balance of Aerosol
 8 Particles over the São Paulo Metropolitan Area of Brazil, *Aerosol Science and
 9 Technology*, 38:S2, 52-62, DOI: 10.1080/02786820490466756

10 Yum, S. S., Hudson, J. G., Song, K. Y., and Choi, B.-C.: Springtime cloud
 11 condensation nuclei concentrations on the west coast of Korea, *Geophys. Res. Lett.*, 32,
 12 L09814,doi:10.1029/2005GL022641, 2005.

13 Yum, S. S., Roberts, G., Kim, J. H., Song, K. Y., and Kim, D. Y.: Submicron
 14 aerosol size distributions and cloud condensation nuclei concentrations measured at
 15 Gosan, Korea, during the Atmospheric brown clouds East Asian Regional Experiment
 16 2005, *J. Geophys. Res.*, 112, D22S32, doi:10.1029/2006JD008212,2007.

17 Zhang, Q., M. R. Canagaratna, J. T. Jayne, D. R. Worsnop, and J.-L. Jimenez,
 18 2005. Time- and size-resolved chemical composition of submicron particles in
 19 Pittsburgh: Implications for aerosol sources and processes, *J. Geophys. Res.*, 110,
 20 D07S09, doi:10.1029/2004JD004649.

21

22

Supersaturation	0.23%	0.45%	0.68%	0.90%	1.13%
Mean N_{CCN}	1090±328	2202±1035	2776±1331	3175±1503	3570±1695
Activated	0.10±0.05	0.19±0.09	0.23±0.10	0.26±0.11	0.28±0.12

fraction					
----------	--	--	--	--	--

1

2 **Table 1.** Details on the mean measured N_{CCN} values furnished by CCNC for São Paulo
3 from 16th to 31st October 2012. Supersaturation values are estimated considering the
4 air pressure between the operating conditions in São Paulo and that during factory
5 calibration.

Org	NH ₄	SO ₄	NO ₃	Cl	BC
4.81±3.05	0.30±0.27	0.52±0.32	0.37±0.21	0.04±0.04	3.26±2.10

6

7 **Table 2.** Mean concentration (± standard deviation) for Organics, NH₄, Sulfate,
8 Nitrate, Chloride and Black Carbon concentration (in µg/m³) measured in São Paulo
9 from 16th to 31st October 2012.

Supersaturation (%)	$a[-]$	$R^2[-]$	Mean predicted/measured N_{CCN} (± standard deviation)
0.23	1.52	0.44	1.44±0.47
0.45	1.47	0.73	1.47±0.35
0.68	1.58	0.78	1.59±0.34
0.90	1.65	0.80	1.66±0.34
1.13	1.89	0.79	1.91±0.40

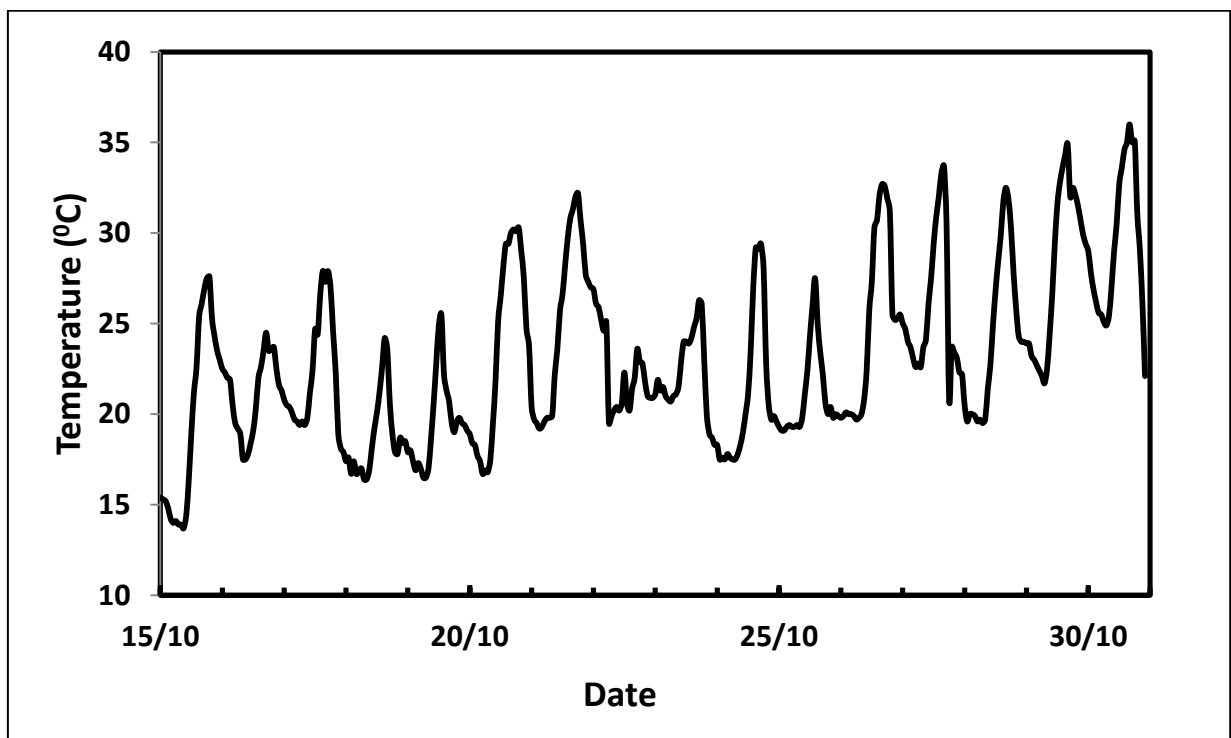
10

11 **Table 3.** a) Details on the predicted vs. measured N_{CCN} considering chemical
12 composition measured by ACSM. a is the slope of the fitted line, R^2 is the square of the
13 correlation coefficient.

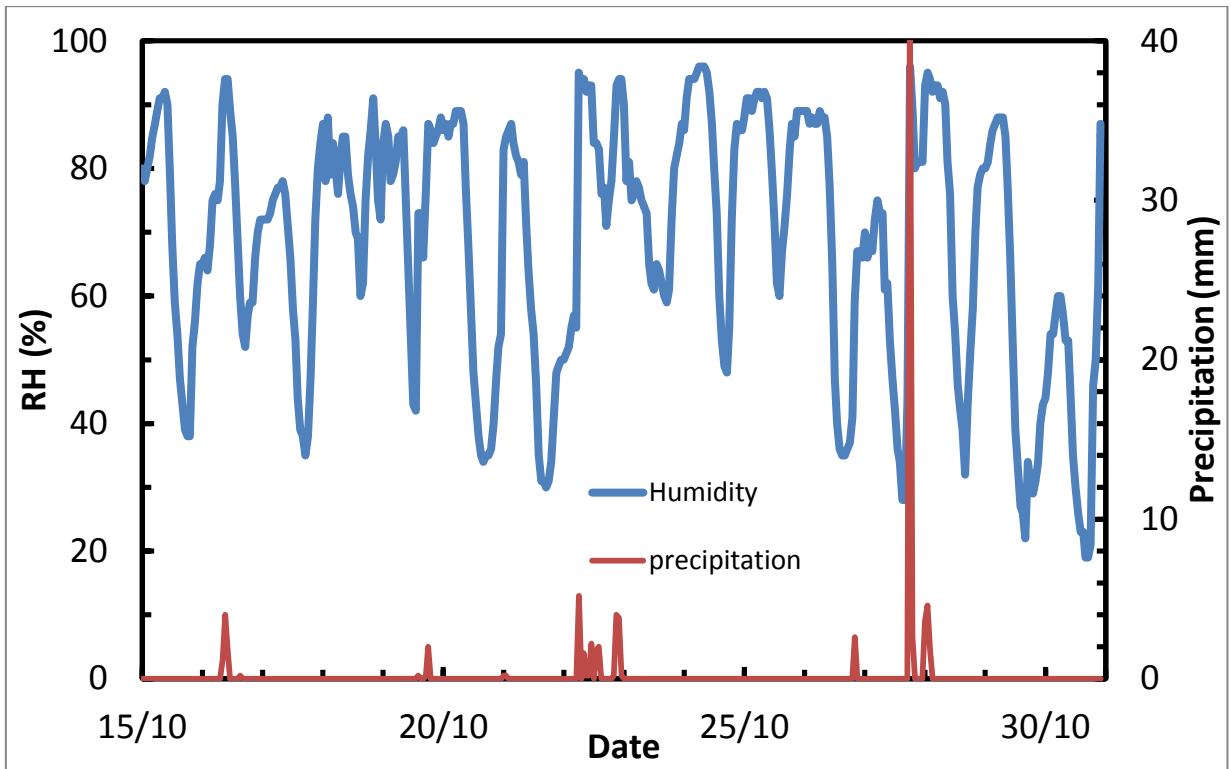
1

Supersaturation (%)	$a[-]$	$R^2[-]$	Mean predicted/measured $N_{CCN} (\pm \text{standard deviation})$
0.23	1.22	0.43	1.14±0.36
0.45	1.00	0.69	1.02±0.25
0.68	1.03	0.76	1.03±0.23
0.90	1.04	0.79	1.04±0.22
1.13	1.03	0.79	1.03±0.22

2 **Table 3. b)** Details on the predicted vs. measured N_{CCN} considering mean chemical size
3 dependency furnished by MOUDI+PIXE and ACSM hourly chemical composition.

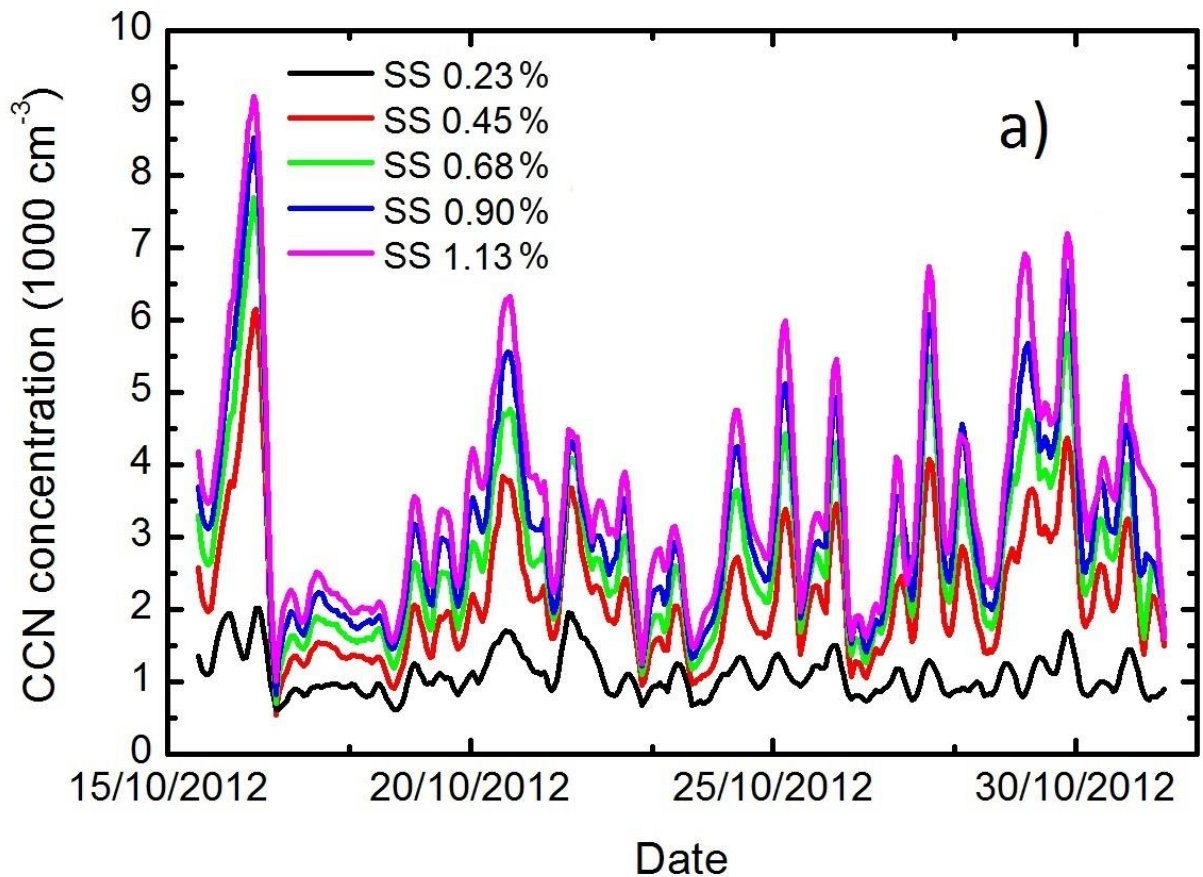


4

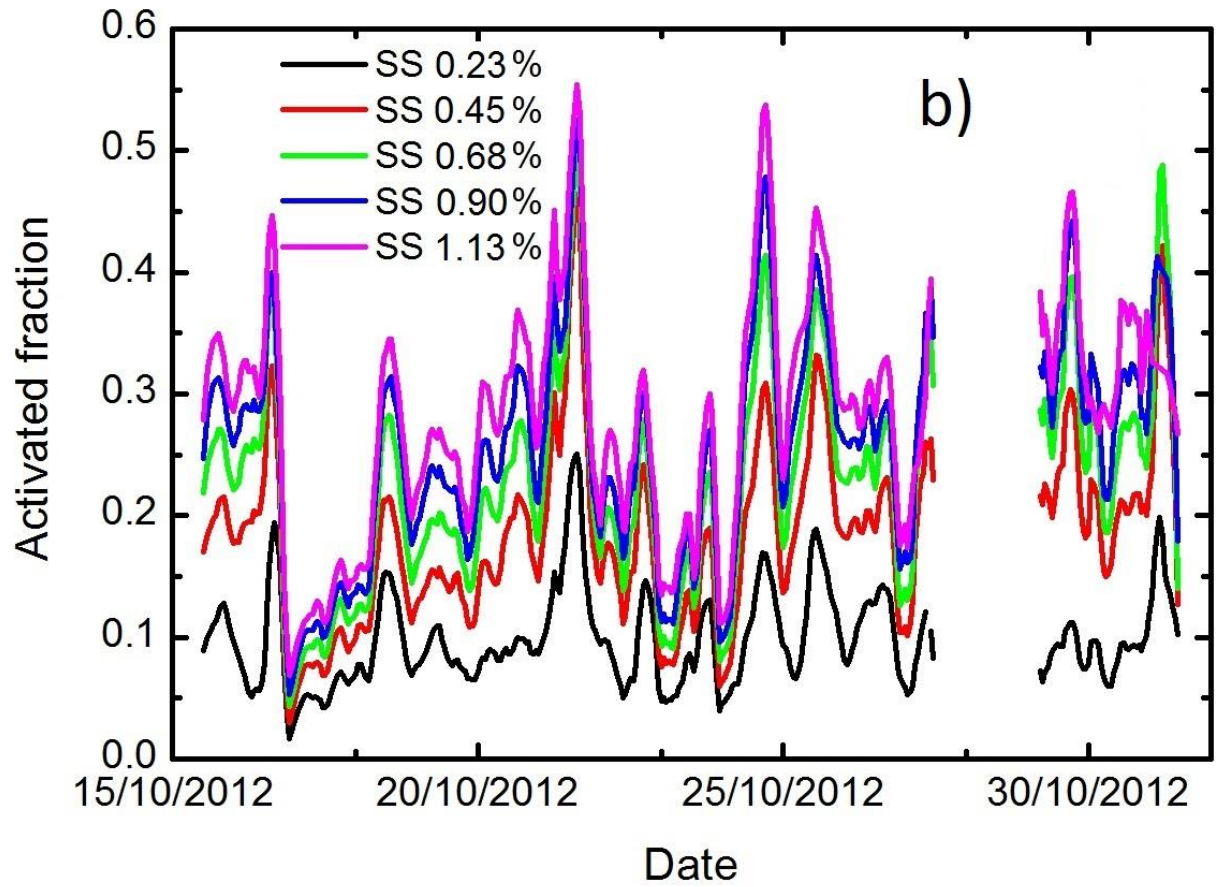


1

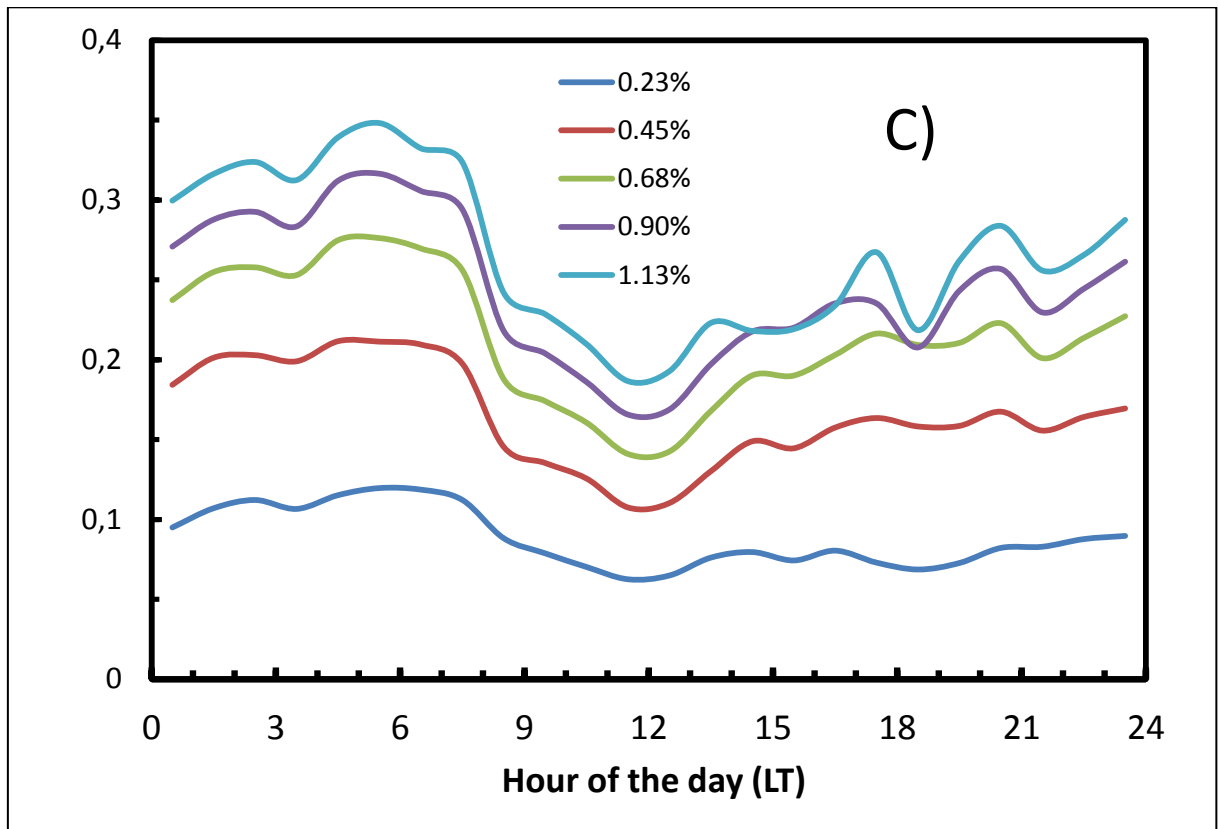
2 Figure 1. Time series of the (a) temperature and (b) RH and precipitation at the
 3 sampling site during the studied period.



4



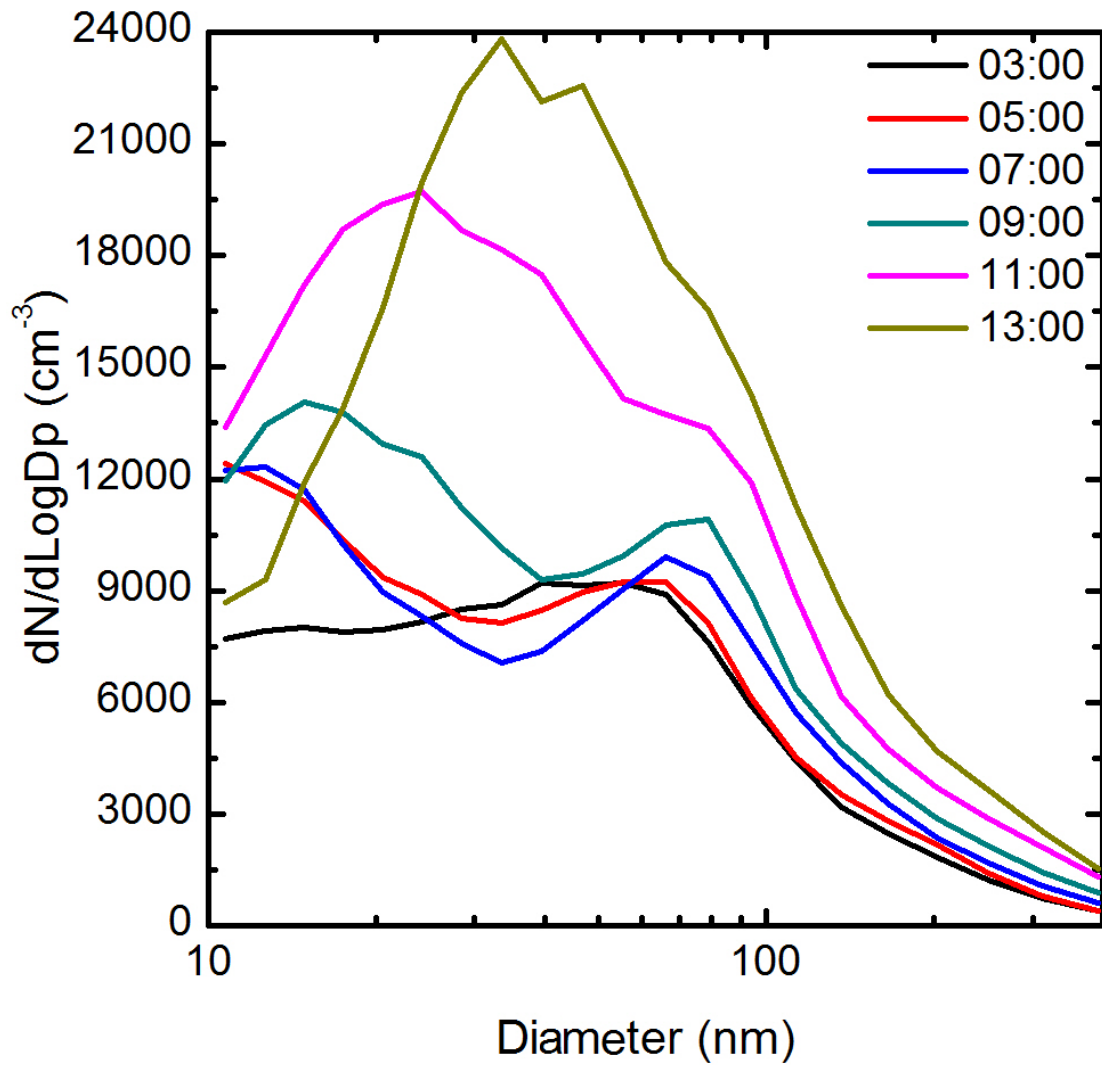
1



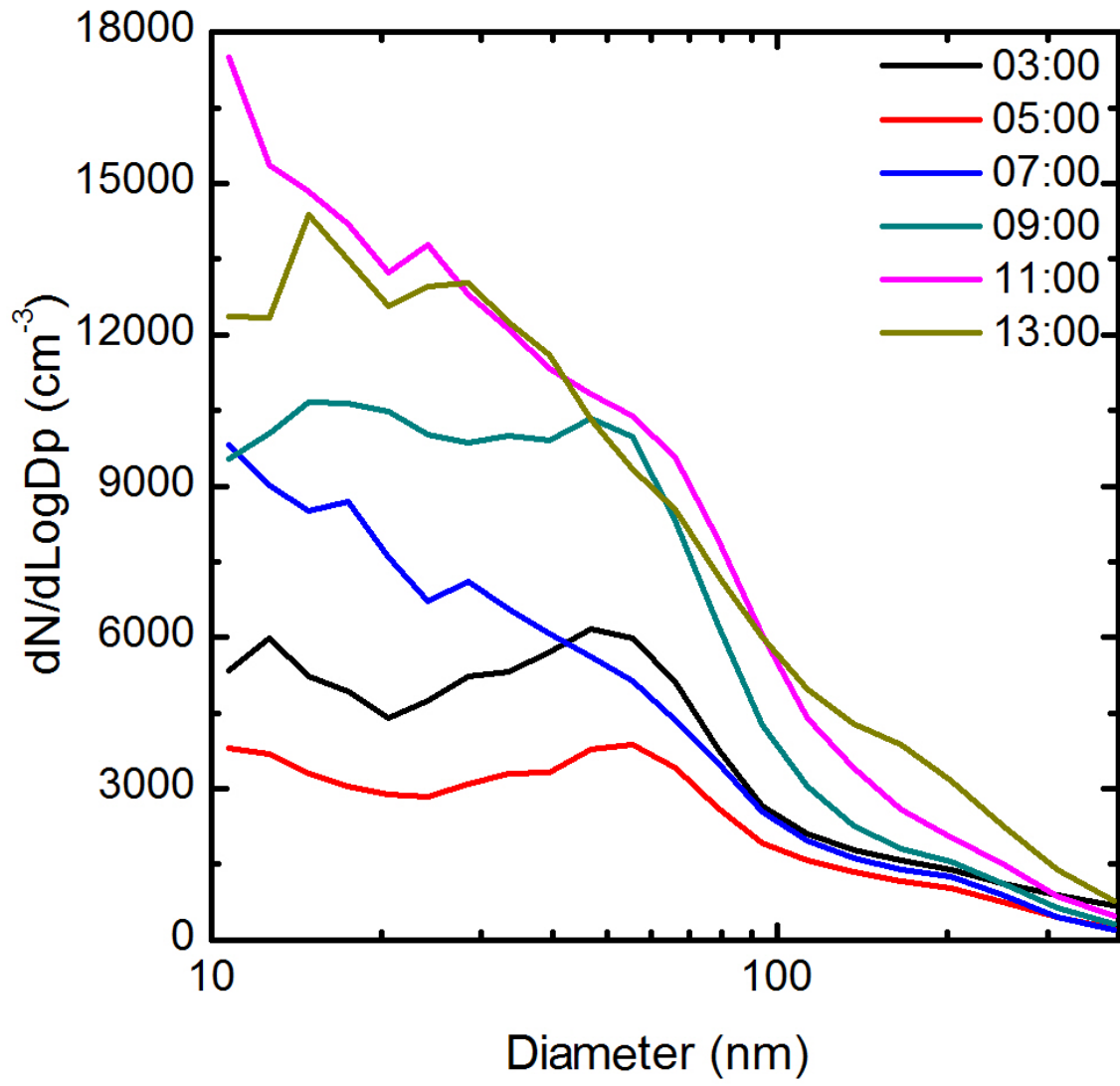
2

3

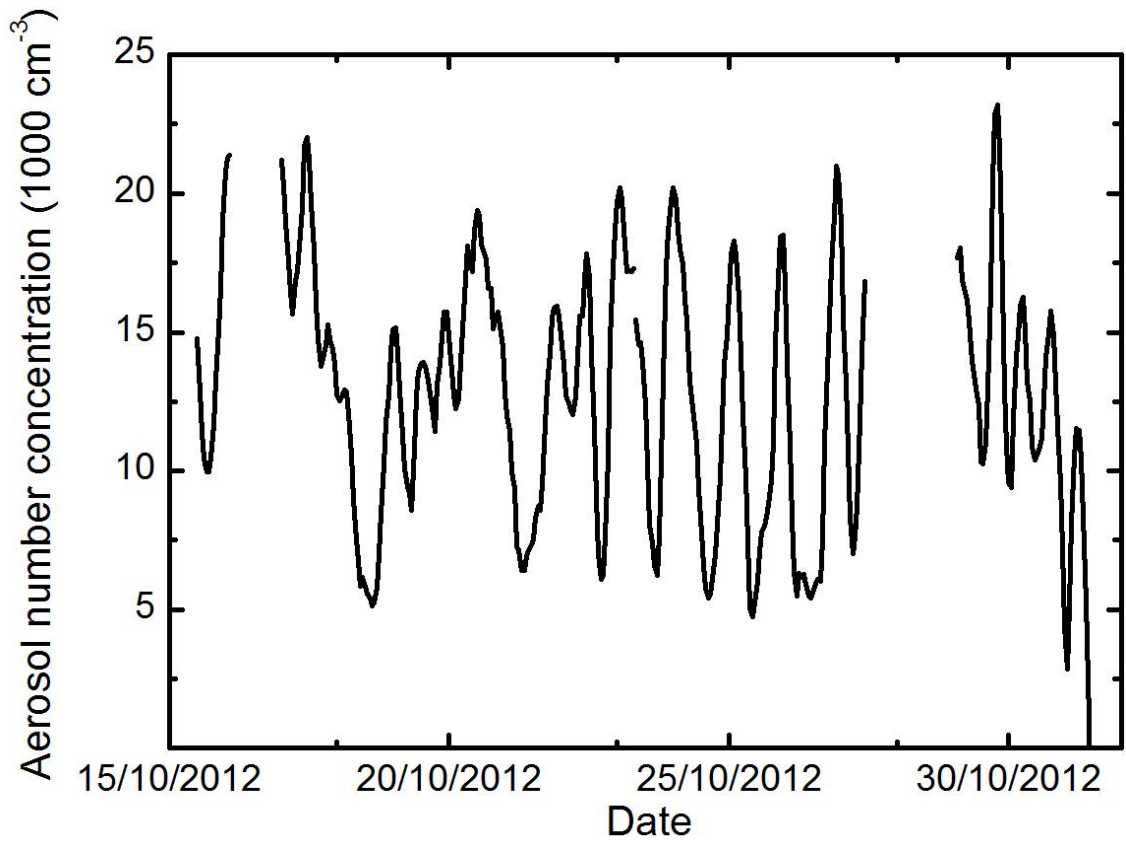
1 Figure 2. Time series of (a) CCN number concentration, (b) the activated fraction
2 (#CCN/N10–500) and (c) the mean hourly averaged over the whole period. The
3 different colours represent the different supersaturations (SS).



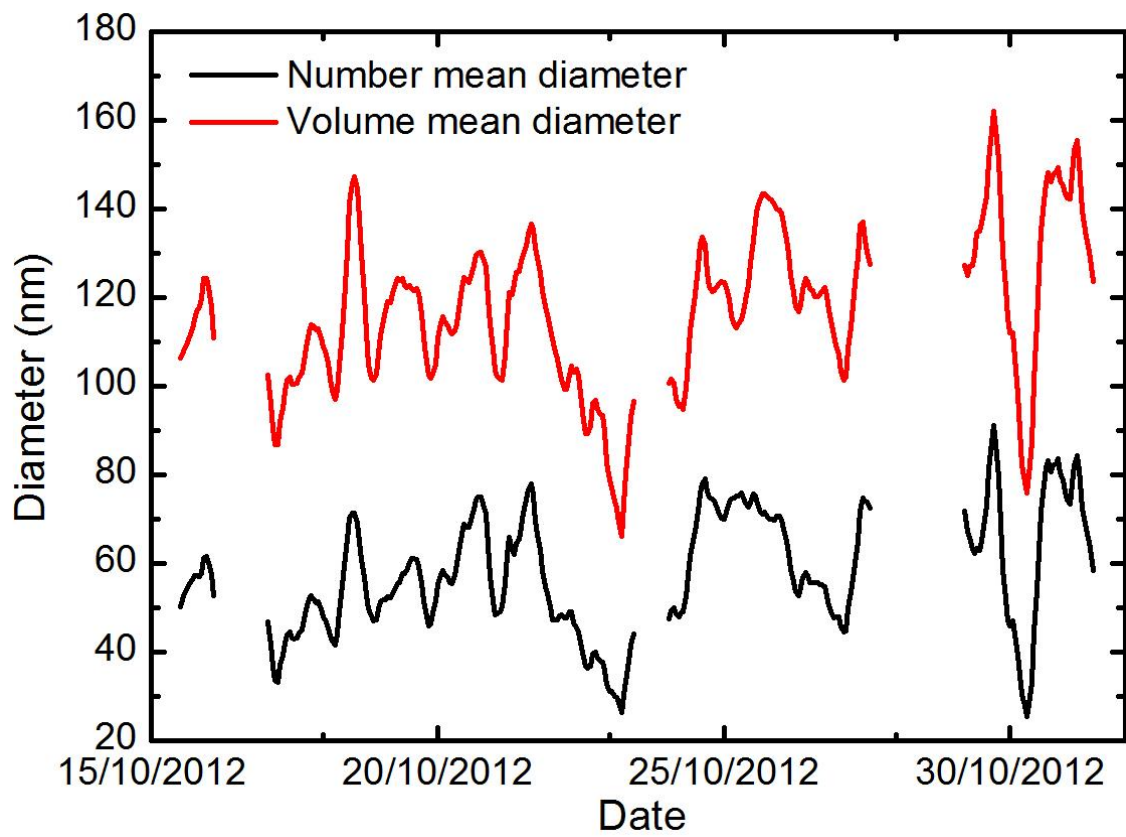
4



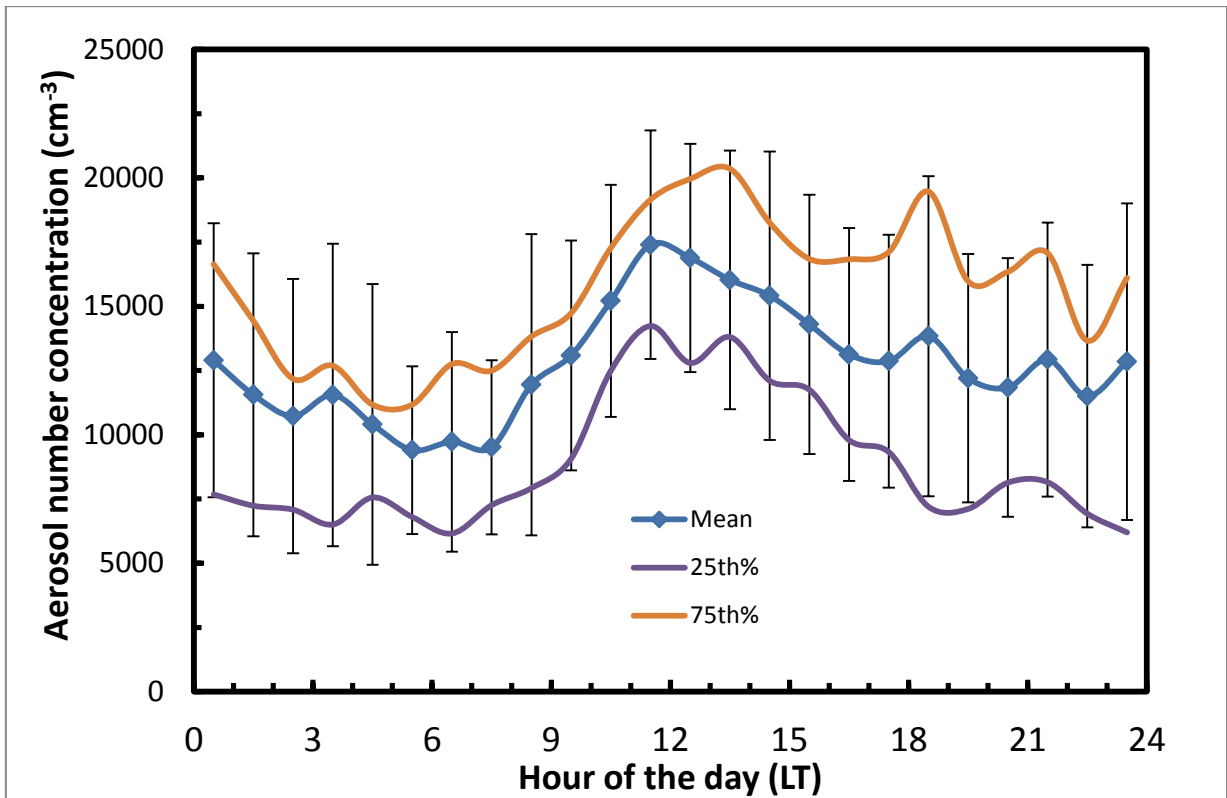
1



1

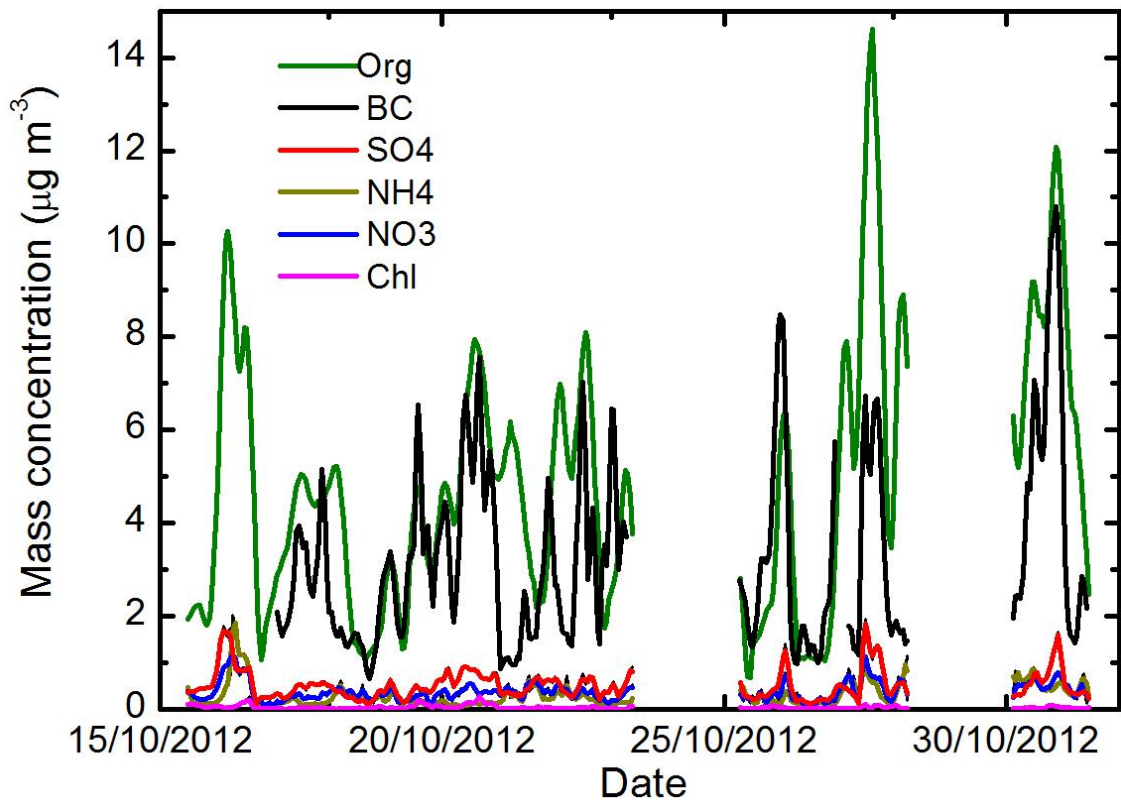


2

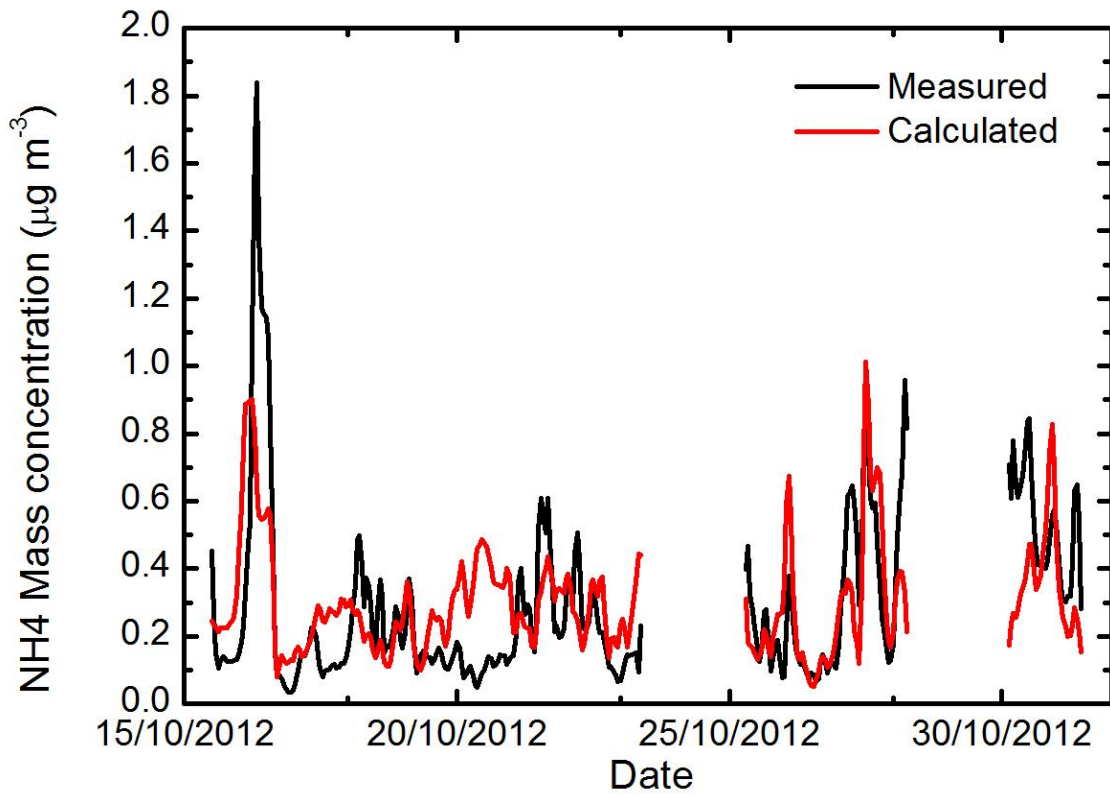


1

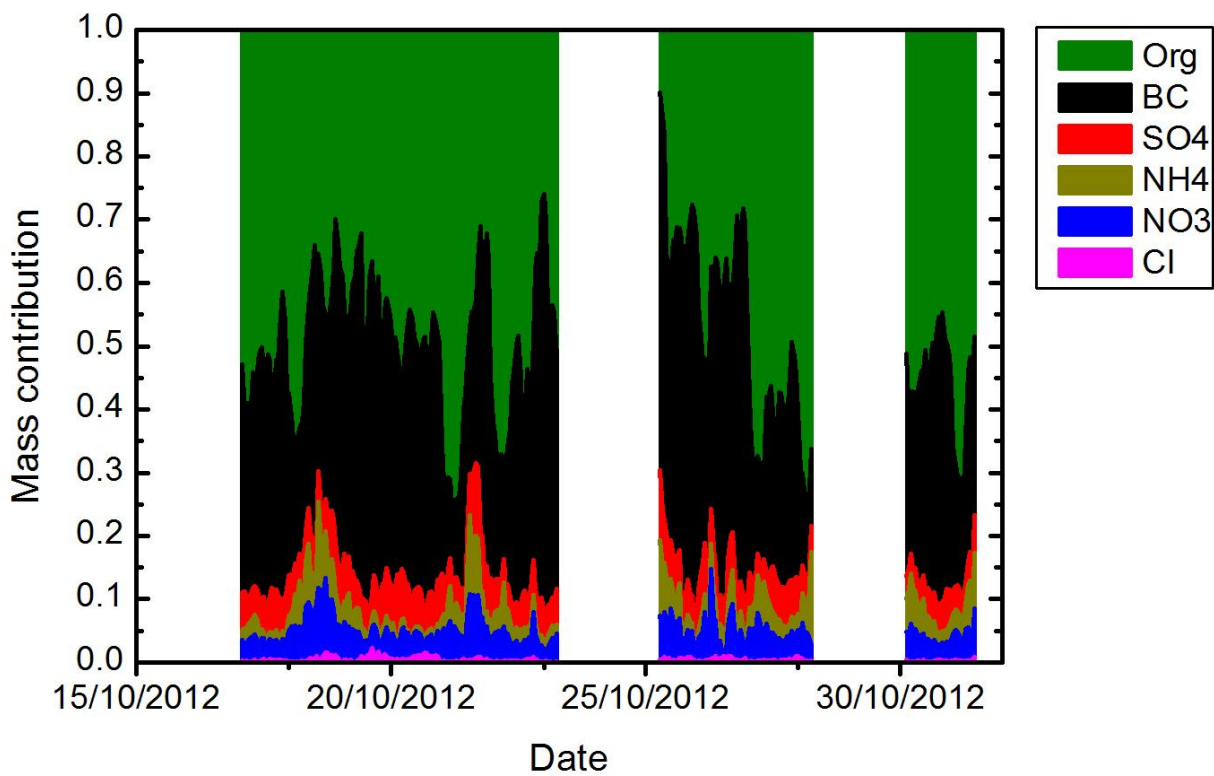
2 Figure 3. (a) aerosol size distribution during 16 October 2012 in SP (b) the same as in
 3 (a), but for 17 October (c) Total particle concentration form 10 nm to 500 nm (d) mean
 4 particle diameter and mean particle volumetric diameter, and (e) total particle number
 5 concentration. 25th% and 75th% refer to the first and third quartile while bars represent
 6 standard deviation.



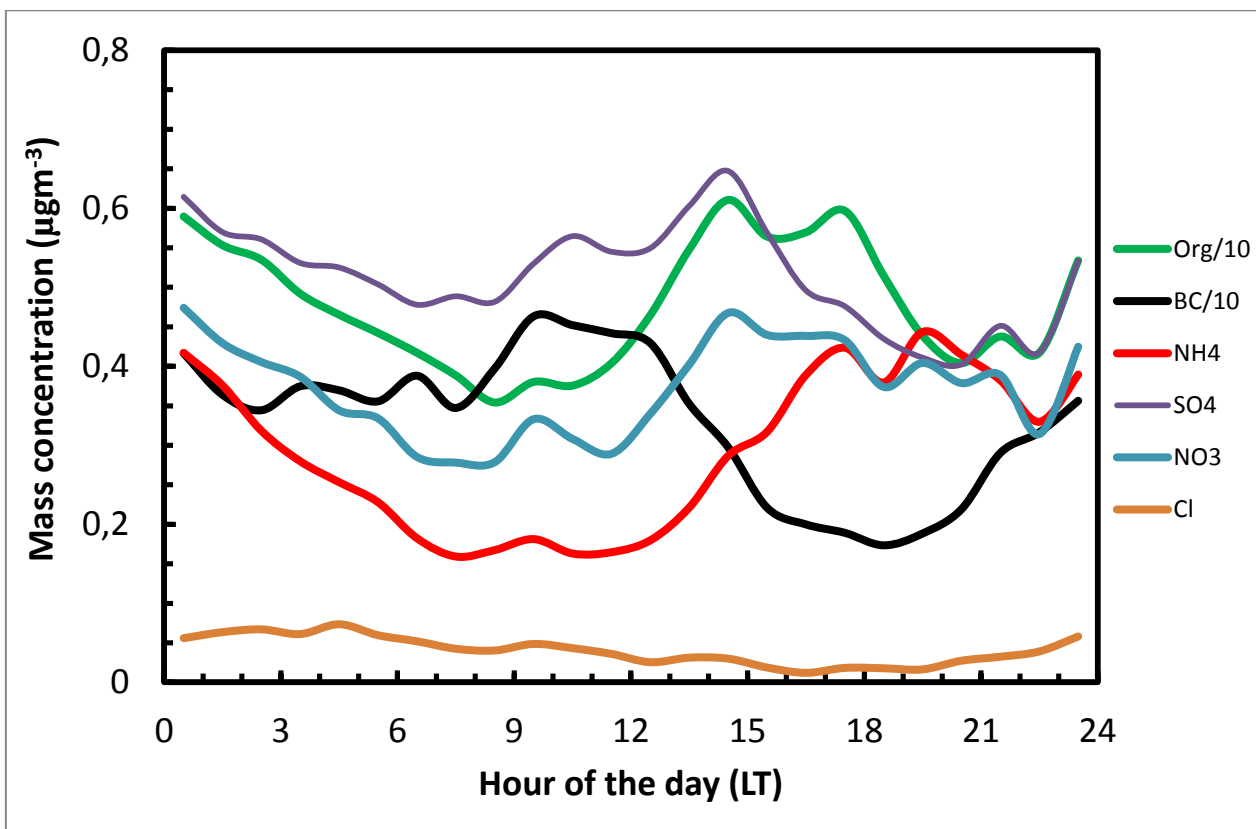
1



2



1

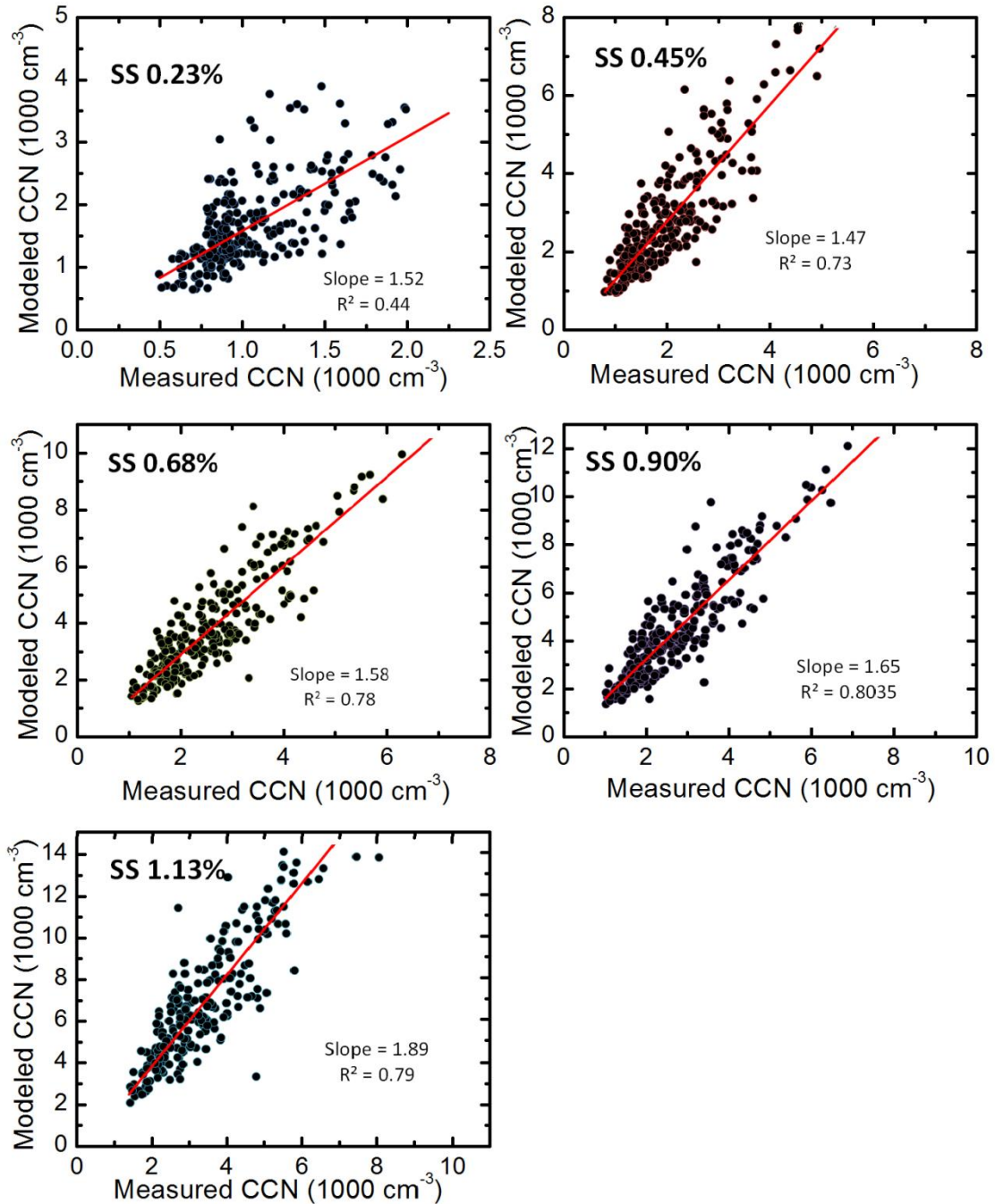


2

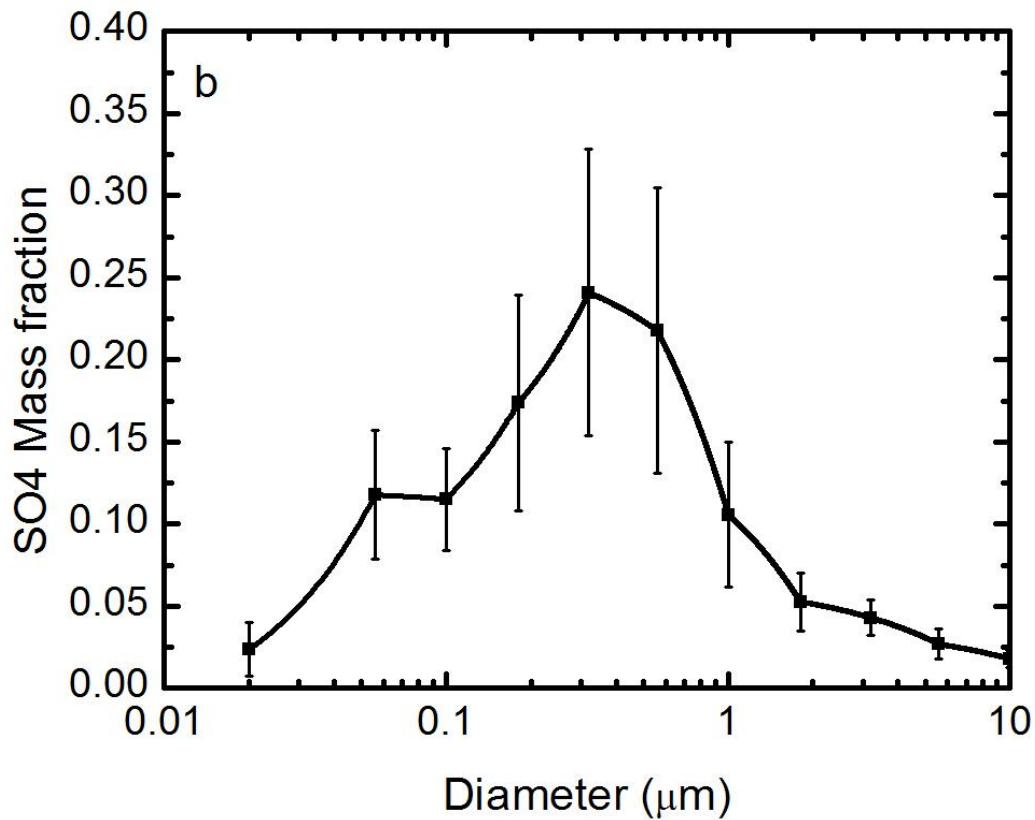
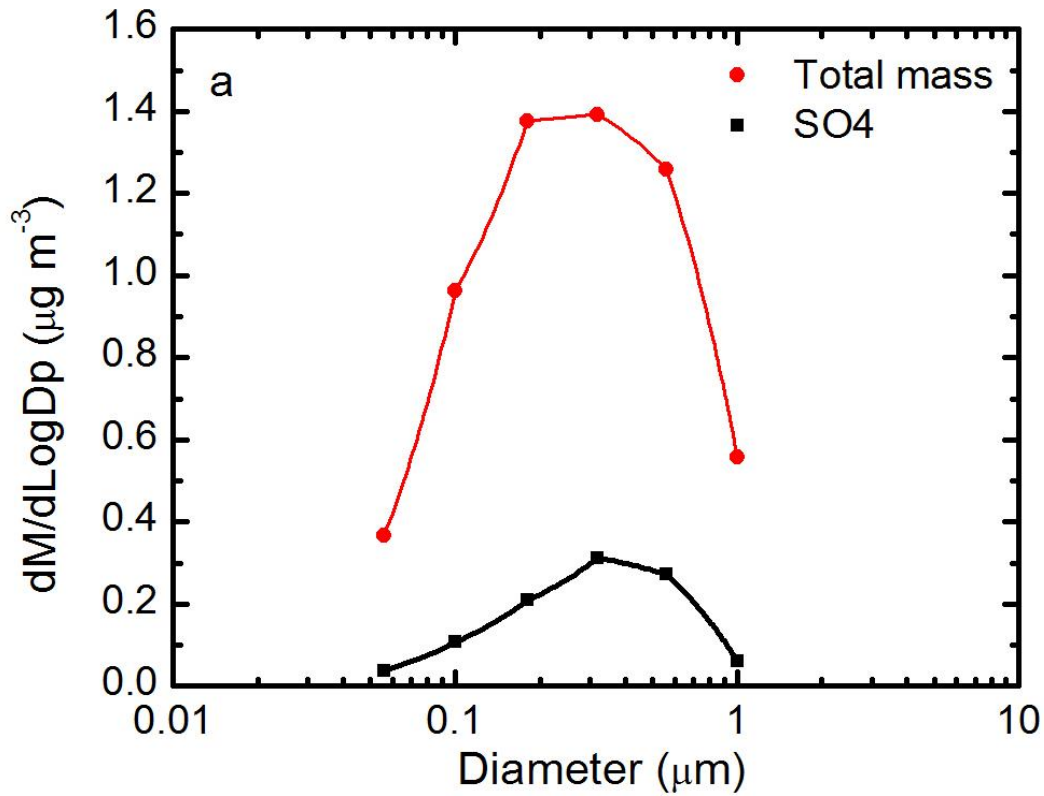
3 Figure 4. Chemical composition of the aerosol, measured by the ACMS and the MAAP.

4 (a) mass concentration of the individual species, (b) mass concentration of the measured

- 1 NH_4 and the calculated amount needed for complete neutralization, (c) the mass
- 2 fractions of the organics, NH_4 , NO_3 , SO_4 and black carbon, and (d) the mean aerosol
- 3 chemical composition as a function of local time



- 4
- 5 Figure 5. Comparison of modeled and measured CCN concentrations using internal
- 6 mixing for the 5 estimated supersaturation (0.23%, 0.45%, 0.68%, 0.90%, and 1.13%).

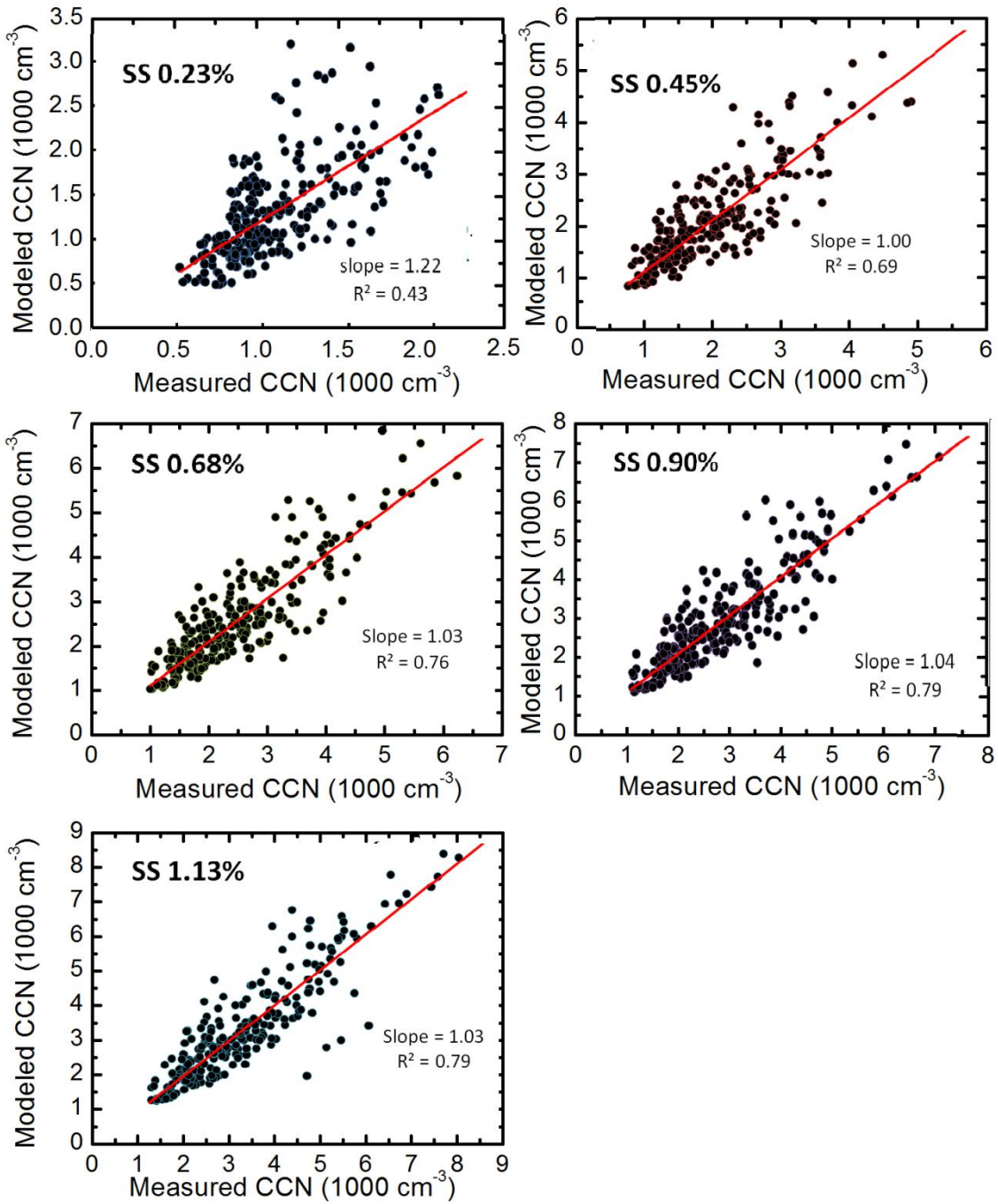


1

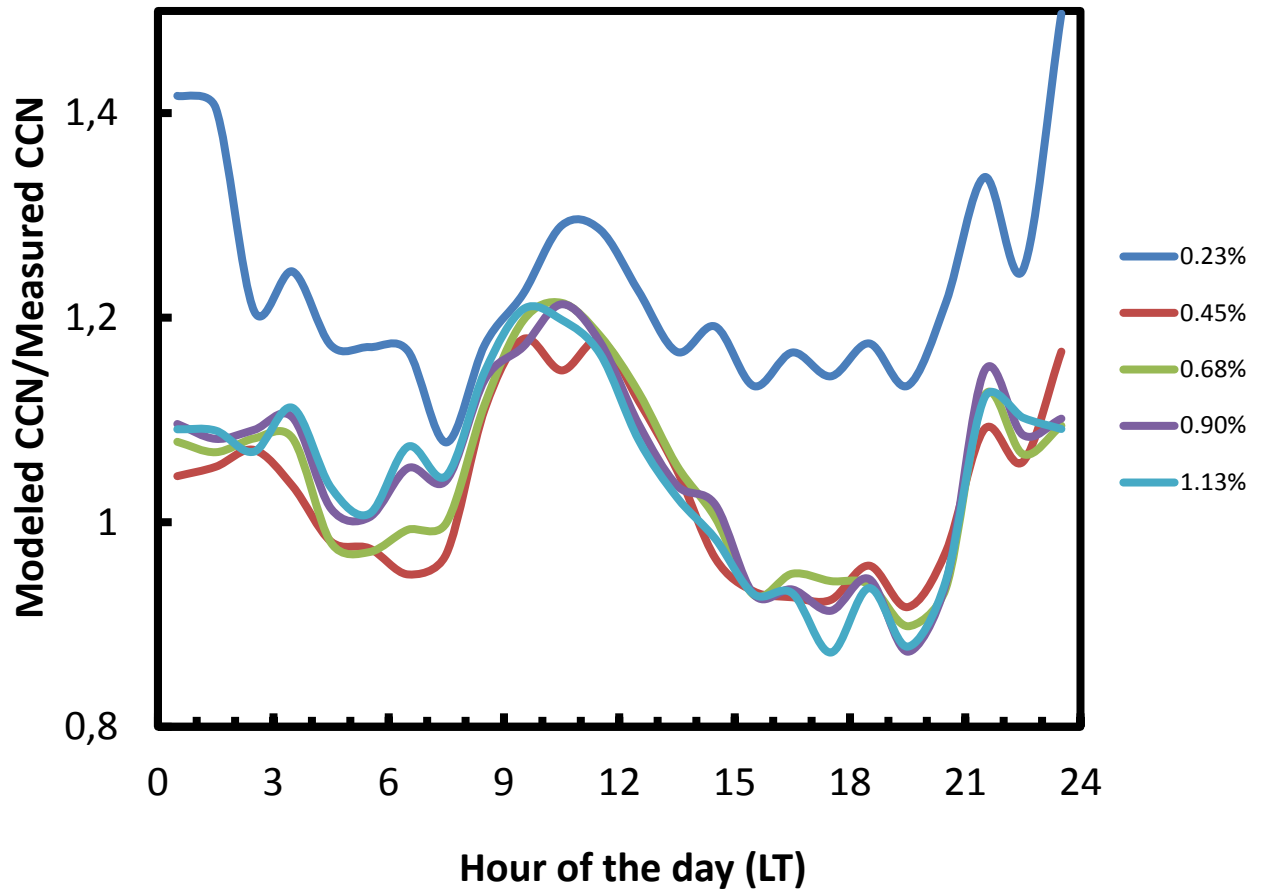
2 Figure 6. Mean value of (a) $dM/d\log d$ ($\mu\text{g}/\text{m}^3$) for the period of 15th August to 5th

3 September 2012 and b) SO_4 mass fraction for the same period. The mass distribution

- 1 was obtained using MOUDI samples, while chemical composition was obtained after
- 2 PIXE analysis. See text for more details



- 3
- 4 Figure 7) Same as Figure 5, but using the size dependence based on MOUDI+PIXE
- 5 analysis



1

2 Figure 8. Mean value of Modeled N_{CCN} /Observed N_{CCN} for different supersaturation as
 3 a function of local time